nature communications

Article

https://doi.org/10.1038/s41467-025-62395-5

Viral proteins suppress rice defenses by boosting OsTSN1 RNA decay via phase separation and multimerization

Received: 2 December 2024

Accepted: 18 July 2025

Published online: 12 August 2025

Check for updates

Ming Zeng[1,7], Shuai Fu[1,2,7], Youping Xu[3], Liyan Li[1], Dan Wang[1], Shi-bo Gao[1], Lianshun Zheng[1], Yunge Zhang[1], Cui Zhang[1], Shifang Fei[1,4], Xuan Ye[1], Lele Chen[1], Yaqin Wang[1], Tong Zhang[5] ✉, Xueping Zhou[1,6] ✉ & Jianxiang Wu[1,4] ✉

Liquid-liquid phase separation (LLPS) forms membraneless condensates crucial for plant stress responses. However, how plant viruses utilize LLPS to escape host immunity remains largely unexplored. Here, we show that P6 protein encoded by southern rice black-streaked dwarf virus (SRBSDV) undergoes LLPS. P6 interacts with OsTSN1 to form the P6-OsTSN1-containing droplets co-localized with stress granules (SGs). Within these droplets, P6 enhances OsTSN1 nuclease activity via promoting its multimerization to degrade transcripts with G-A-rich motifs of two transcription factors (TFs), OsNAC15 and OsLHY. These two TFs regulate the transcription of *OsJAZ6*, *OsJAZ12*, and *OsATG8C*, key components of jasmonic acid (JA)- and autophagy-associated defense pathways. Furthermore, the degradation of *OsNAC15* and *OsLHY* transcripts in P6-OsTSN1-containing droplets weakens JA- and autophagy-mediated defenses in rice, facilitating SRBSDV infection. Additionally, similar to SRBSDV P6, intrinsically disordered region (IDR)-containing RNA silencing suppressors encoded by rice black-streaked dwarf virus and rice stripe virus, also interact with OsTSN1, promoting the degradation of OsNAC15 and OsLHY transcripts to enhance viral infection. Our findings indicate that OsTSN1 acts as a central positive regulator of virus infection in rice, convergently co-opted by viruses. These insights help us to better understand the roles of LLPS and OsTSN1 in virus infection in rice.

Plant viruses often pose serious threats to food security, resulting in huge yield and economic losses every year[1]. Rice is a major food crop in many countries and is vulnerable to many arbovirus infections[2,3]. Among these arboviruses, southern rice black-streaked dwarf virus (SRBSDV), a member of the genus *Fijivirus*, family *Reoviridae*, transmitted in a persistent-propagative manner by *Sogatella furcifera* (white-backed planthopper, WBPH), is currently the most destructive virus in paddy fields[4]. SRBSDV contains ten double-stranded genomic RNAs and encodes at least 13 proteins[5]. The SRBSDV P1 protein is known as a putative RNA-dependent RNA polymerase (RdRP), and the

[1]State Key Laboratory of Rice Biology and Breeding, Zhejiang Key Laboratory of Biology and Ecological Regulation of Crop Pathogens and Insects, Institute of Biotechnology, Zhejiang University, Hangzhou, Zhejiang, P.R. China. [2]Research Center for Life Sciences Computing, Zhejiang Lab, Hangzhou, China. [3]Analysis Center of Agrobiology and Environmental Sciences, Zhejiang University, Hangzhou, Zhejiang, P.R. China. [4]Hainan Institute of Zhejiang University, Sanya, P.R. China. [5]Guangdong Province Key Laboratory of Microbial Signals and Disease Control, College of Plant Protection, South China Agricultural University, Guangzhou, China. [6]State Key Laboratory for Biology of Plant Diseases and Insect Pests, Institute of Plant Protection, Chinese Academy of Agricultural Sciences, Beijing, P.R. China. [7]These authors contributed equally: Ming Zeng, Shuai Fu. ✉e-mail: zhangtong@scau.edu.cn; zzhou@zju.edu.cn; wujx@zju.edu.cn

P3 protein is a putative capping enzyme. The P2 and P4 proteins are the putative capsid shell and spike proteins, while the P8 and P10 are the core and major outer capsid proteins, respectively[6,7]. Among the presumed nonstructural proteins, P5-1, P6, and P9 have been reported to be involved in virosome formation[8,9]. The P7-1 protein has been shown to form tubular structures to facilitate virus cell-to-cell transmission[10,11].

Other arboviruses causing severe damage to rice production in East and South Asia are rice black-streaked dwarf virus (RBSDV), also a member of the genus *Fijivirus*, and rice stripe virus (RSV), which belongs to the genus *Tenuivirus*. Unlike SRBSDV, these two viruses are transmitted in a persistent-propagative manner by *Laodelphax striatellus* (small brown planthopper, SBPH)[12,13].

During the co-evolutionary arms race between plants and viruses, plants have evolved sophisticated immune systems to defend against viral infections[14]. These immune systems include RNA interference, RNA decay, autophagy, and JA-, SA-, and other hormone-related signaling pathways[15–21]. Recently, many reports have indicated that biomolecular condensates are involved in various plant immune responses[22–24]. These biomolecular condensates comprising diverse proteins and RNAs are formed via liquid–liquid phase separation (LLPS)[25], exemplified by stress granules (SGs), processing bodies (PBs), siRNA bodies, and Cajal bodies[26]. Biomolecular condensates co-operate with one another to play pivotal roles in plant growth and immune defenses against various stresses[27], including stress induced by virus infections[28]. Recent evidences indicate that PBs are enriched with RNA-cognate proteins associated with multiple stress responses, immune regulation, and ethylene signaling[29]. Conversely, viruses can exploit biomolecular condensates to suppress plant immunity and/or benefit viral processes[30]. Several reports have indicated that PB components are co-opted by viruses to weaken host RNA interference capability and maintain viral replication[31,32]. The RNA silencing suppressor of potato virus A (PVA) has the ability to recruit host RNA-binding proteins to form RNA-protein granules, which regulate PVA translation[33]. Additionally, the nuclear shuttle proteins (NSP) of abutilon mosaic virus (AbMV) and pea necrotic yellow dwarf virus (PNYDV) have been reported to interfere with the formation of SGs by interacting with G3BP to modulate host stress response and favor viral protein translation[34].

Tudor staphylococcal nucleases (TSNs), as an RNA-binding protein and ribonuclease, characterized by four unique tandem SN domains in the N-terminus and a Tudor-SN domain in the C-terminus, are evolutionarily conserved across most eukaryotic organisms[35]. They are an essential component of SGs in animals and plants[36–38]. In animals, TSNs play critical roles in various biological processes, including transcription regulation[39,40], endonuclease-mediated miRNA decay[41], cleavage of hyper-edited dsRNA[42], RNA silencing regulation[43] and RNA splicing[44]. However, the biological functions of TSNs in plants are not identical to those in animals[35]. Rice TSN has been identified as a cytoskeleton-associated RNA-binding protein that transports mRNAs of storage proteins to the cortical endoplasmic reticulum during rice endosperm development[45–47]. Arabidopsis TSNs act as scaffolds for SGs and are involved in mRNA catabolism and signal transduction during heat stress[48,49]. Under salt stress, Arabidopsis TSNs help maintain cell homeostasis by regulating mRNA levels of *GA20ox3* and stabilizing stress-related mRNAs[50,51]. Recently, the Arabidopsis TSN protein has been identified in the proteome of the processing body[52]. Additionally, TSN in Norway spruce is proteolytically cleaved and inactivated by metacaspase during developmental and stress-induced cell death[53]. However, the role of TSNs in regulating rice responses to abiotic and biotic stresses has received limited attention.

As a nonstructural protein of SRBSDV, P6 has been shown to function as a silencing suppressor during virus infection[4]. Recently, P6 has also been reported to modify ethylene signaling in rice plants, affecting insect feeding behavior[54]. Here, we provide evidence to define that SRBSDV P6 can undergo LLPS to form droplets with OsTSN1 and localize in SGs. Within these droplets, autophagy-related *OsNAC15* and JA-related *OsLHY* gene transcripts are highly enriched. As transcription factors (TF), OsNAC15 and OsLHY activate the autophagy- and JA-related immune pathways in rice plants by regulating the transcription of downstream genes *OsATG8C*, *OsJAZ6* and *OsJAZ12*. SRBSDV P6 can enhance the nuclease activity of OsTSN1 by promoting its multimerization to degrade *OsNAC15* and *OsLHY* transcripts, impairing rice host immune response and facilitating virus infection. Notably, we demonstrate that RBSDV- and RSV-encoded RNA silencing suppressors also undergo LLPS to form droplets with OsTSN1, and promote OsTSN1 multimerization to facilitate virus infection. Collectively, these findings provide insights into the role of RNA decay in the infection process of rice viruses and show that this process is convergently co-opted by rice viruses.

Results

SRBSDV P6 undergoes liquid–liquid phase separation

To investigate the function of SRBSDV P6, we first analyzed the subcellular location of GFP-P6 in *Nicotiana benthamiana* leaf cells and rice protoplasts. Unlike the dispersed cytoplasmic distribution of GFP, GFP-P6 accumulated mainly in granules in the cytoplasm (Fig. 1a, b). Moreover, GFP-P6 in rice protoplasts was not only granular but also soluble. This observation suggests that P6 may undergo LLPS. Proteins that undergo LLPS often contain intrinsically disordered regions (IDRs)[27]. Analysis of SRBSDV P6 using the Predictor of Natural Disordered Regions (PONDR) and Intrinsically Unstructured Protein Predictor (IUPred3) tools showed that it contained three IDRs (Fig. 1c). To investigate whether P6 has liquid-like characteristics, we performed a fluorescence recovery after photobleaching (FRAP) assay, and the result showed that GFP-P6 recovered well over time in the photobleached areas (Fig. 1d, e). Additionally, the shape and size of GFP-P6-formed droplets were dynamic and adjacent droplets fused together to form large droplets (Fig. 1f). Using purified prokaryotically expressed RFP-P6, we found that RFP-P6-formed droplets in the presence of 8% PEG-8000, and as the protein concentration increased, the size of RFP-P6 droplets also increased (Fig. 1g). However, with increasing concentrations of KCl, the size of RFP-P6 droplets gradually decreased (Fig. 1h). Also in this case, FRAP showed that, after photobleaching, the fluorescence signal of RFP-P6 droplets recovered gradually (Fig. 1i, j). To determine which IDR in the P6 is responsible for its phase separation, we truncated P6 into two parts: the N-terminal part (1–350 aa) contained IDR1, and the C-terminal part (351–793 aa) contained IDR2 and IDR3 (Fig. 1c and Supplementary Fig. 1a). Analysis of these two truncated mutants in *N. benthamiana* leaf cells showed that mCherry-C-P6, but not mCherry-N-P6, formed liquid-like granules (Supplementary Fig. 1b). We then divided the C-P6 into two smaller regions: C-P6a (351-550aa with IDR2) and C-P6b (551–793 aa with IDR3) (Supplementary Fig. 1a). mCherry-C-P6b could form droplets in vivo, but mCherry-C-P6a could not (Supplementary Fig. 1b). The droplets of mCherry-C-P6b in photobleached areas recovered rapidly (Supplementary Fig. 1c, d), indicating that the IDR3 of P6 is likely responsible for the phase separation. Furthermore, we compared the purified prokaryotically expressed RFP-IDR3 with RFP-P6$^{\Delta IDR3}$ and found that RFP-IDR3 formed droplets in vitro, but RFP-P6$^{\Delta IDR3}$ did not (Fig. 1k). The fluorescence signal from the photobleached RFP-IDR3 droplets recovered gradually during the FRAP assay (Fig. 1l, m). Taken together, these findings demonstrate that SRBSDV P6 undergoes LLPS, for which its IDR3 domain is required.

SRBSDV P6 recruits OsTSN1 to droplets via interaction

Some virus-encoded proteins can recruit host nucleic acids and proteins through the formation of droplets[32,55]. To investigate whether host proteins are also recruited by P6 into its droplets, we performed a co-immunoprecipitation (Co-IP) assay using a P6-specific monoclonal antibody. Analysis of the Co-IP products through SDS-PAGE showed that,

https://doi.org/10.1038/s41467-025-62395-5

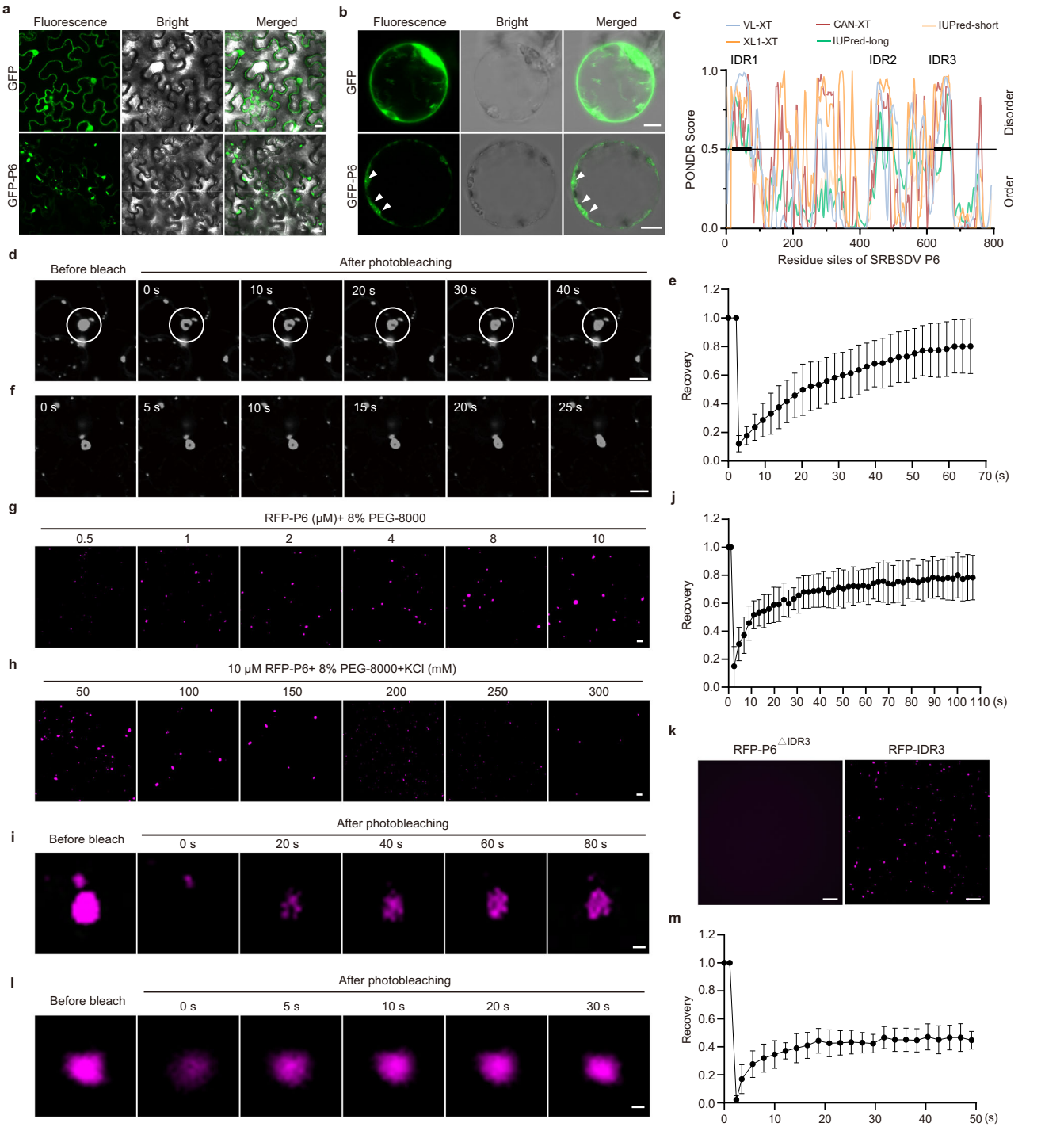

Fig. 1 | SRBSDV P6 undergoes LLPS in vivo and in vitro. a Subcellular localization of SRBSDV P6 in *N. benthamiana* leaf cells at 2 days post agroinfiltration (dpa). GFP alone was used as the control. Scale bar, 20 μm. **b** Subcellular localization of SRBSDV P6 in rice protoplasts at 12 h post transfection. GFP alone was used as a control. White arrows indicate droplets. Scale bar, 5 μm. **c** Disorder profiles of P6 were determined using multiple computational predictors, including: (i) VL-XT, XL1-XT, and CAN-XT from the Predictor of Natural Disordered Regions (PONDR; http://www.pondr.com/), and (ii) IUPred-long and IUPred-short from the Intrinsically Unstructured Protein Predictor (IUPred3; https://iupred3.elte.hu/). Thick black lines indicate IDRs. **d** FRAP assay showing the GFP-P6-formed droplets in the cytoplasm of *N. benthamiana* leaf cells. White circles indicate the photobleached areas. 0 s–40 s indicate the times after photobleaching pulse. Scale bar, 10 μm. **e** Recovery curve of the photobleached GFP-P6 droplets in the cytoplasm. The data are the means ± SD ($n = 12$ droplets). **f** The fusion between two GFP-P6-formed droplets in cells was captured through Confocal Time-lapse Microscopy. Scale bar, 10 μm. **g** An in vitro droplet formation assay using different concentrations of purified prokaryotically expressed RFP-P6. Scale bar, 10 μm. **h** In vitro formation of RFP-P6 droplets in different concentrations of KCl. Scale bar, 10 μm. **i** FRAP assay showing the recovery of a photobleached RFP-P6 droplet in vitro. Scale bar, 1 μm. **j** Recovery curve of photobleached RFP-P6 droplets in vitro. The data are the means ± SD ($n = 12$ droplets). **k** Confocal images showing the phase separation of RFP-P6$^{\triangle IDR3}$ and RFP-IDR3 in vitro. Scale bar, 10 μm. **l** FRAP assay showing the recovery of the photobleached RFP-IDR3 droplets in vitro. Scale bar, 1 μm. **m** Recovery curve of the photobleached RFP-IDR3 droplets. The data are the means ± SD ($n = 12$ droplets). Experiments in (**a**, **b**, **g**, **h**, and **k**) were repeated three times with similar results.

https://doi.org/10.1038/s41467-025-62395-5

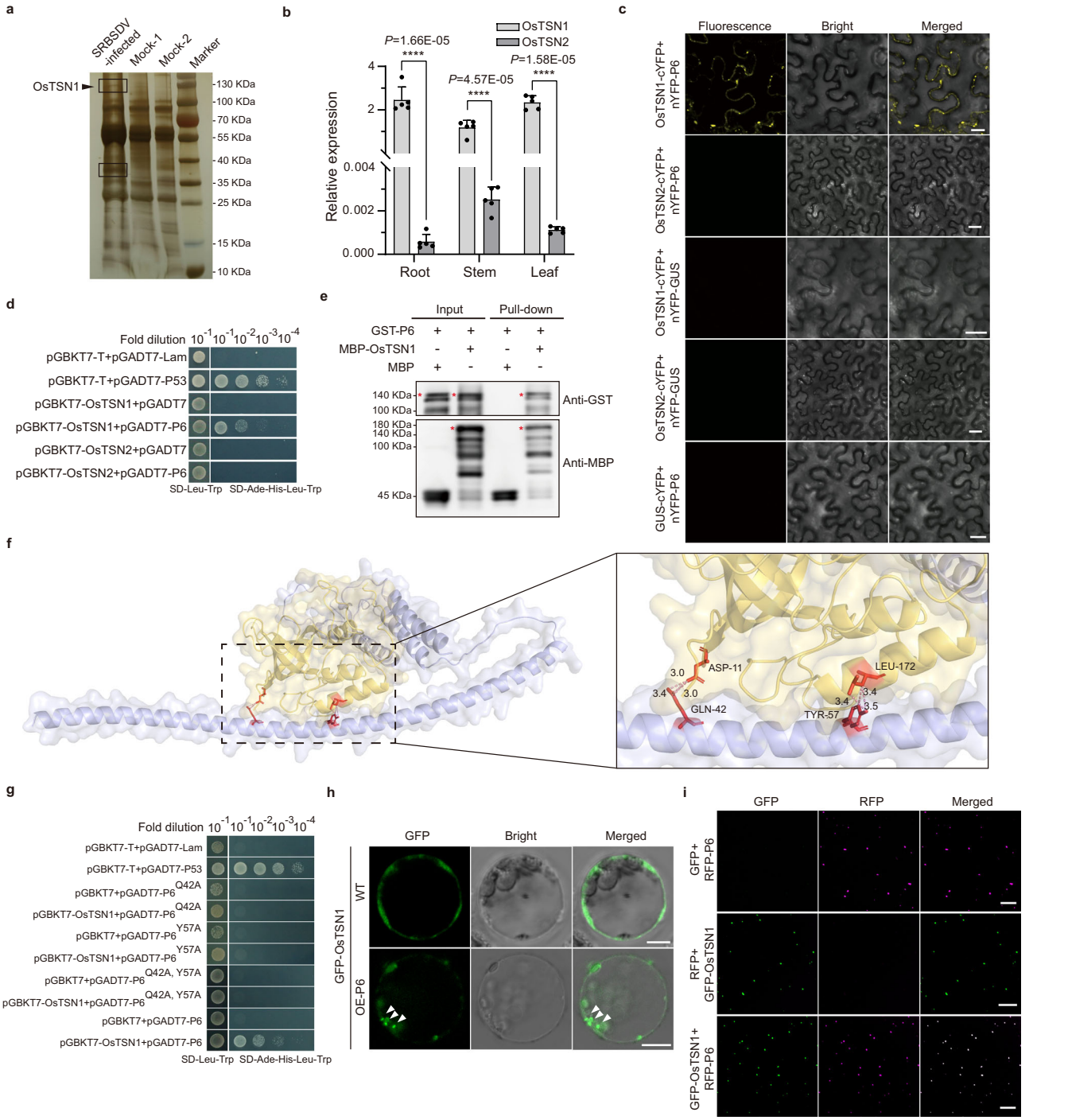

Fig. 2 | OsTSN1 interacts with SRBSDV P6 to form droplets. a A silver-stained SDS-PAGE gel showing P6 co-immunoprecipitated products. Black boxes indicate unique protein bands in SRBSDV-infected rice plants. **b** Results of RT-qPCR assays showing the transcription levels of *OsTSN1* and *OsTSN2* in roots, stems, and leaves of rice. Data are the means ± SD from five independent biological replicates, determined using a two-tailed Student's *t* test. ****$P < 0.0001$. **c** A BiFC assay result showing the interaction between the P6 and OsTSN1 but not OsTSN2 in *N. benthamiana* leaf cells. Scale bar, 20 μm. **d** Y2H assay showing the interaction between P6 and OsTSN1 or OsTSN2. Yeast cells co-transformed with pGBKT7-T and pGADT7-P53 were used as a positive control, while cells co-transformed with pGBKT7-T and pGADT7-Lam were used as a negative control. **e** Pull-down assay showing the interaction between the P6 and OsTSN1. In this assay, GST-P6 was used to pull down MBP-OsTSN1. The membranes were probed with an anti-GST or an anti-MBP antibody. **f** Predicted structures of the C-P6b (551–793 aa) domain and the OsTSN1-SN3 domain using AlphaFold2 (AF2, https://alphafold.ebi.ac.uk/). The two predicted interaction sites are shown. **g** Y2H assay results showing the interaction site between P6 and OsTSN1. Yeast cells co-transformed with pGBKT7-T and pGADT7-P53 were used as a positive control, while the cells co-transformed with pGBKT7-T and pGADT7-Lam were used as a negative control. **h** Subcellular localization of OsTSN1 in rice protoplasts isolated from wild-type (WT) rice or OE-P6 transgenic plants. White arrows indicate droplets. Scale bar, 5 μm. **i** In vitro co-localization of purified GFP-OsTSN1 and RFP-P6 recombinant proteins. Purified GFP and RFP recombinant proteins served as negative controls. Scale bar, 10 μm. Experiments in (**a**, **c**, **e**, **h**, and **i**) were repeated three times with similar results.

compared to the products from uninfected rice plants, two unique protein bands were found in SRBSDV-infected rice plants (Fig. 2a). These two unique protein bands were collected and subjected to analysis via mass spectrometry (MS). Viral proteins and many host proteins involved in regulating plant growth and responding to stress were found in the MS analysis data (Supplementary Data 1). Interestingly, the Tudor staphylococcal nuclease (OsTSN1, LOC_Os02g32350.1) was highly enriched in the IP-MS-generated datasets, which drew our attention. Structural analysis of OsTSN1 using AlphaFold2 (AF2, https://alphafold.ebi.ac.uk/) revealed that OsTSN1 contained four conserved staphylococcal nuclease (SN) domains and a Tudor-SN domain (Supplementary Fig. 2a). An amino acid sequence alignment using two rice TSN proteins, OsTSN1 and OsTSN2 (LOC_Os04g32960.1), and the TSN proteins from other species resulted in a phylogeny tree showing that plant TSNs are highly conserved (Supplementary Fig. 2b). Expression analyses of *OsTSN1* and *OsTSN2* in rice through RT-qPCR showed that the expression level of *OsTSN1* in rice roots, stems, and leaves is significantly higher than that of *OsTSN2* (Fig. 2b).

To investigate whether P6 could interact with OsTSN1 and OsTSN2, we performed BiFC and Y2H assays. The results indicated that P6 did interact with OsTSN1, but not with OsTSN2 (Fig. 2c, d). Our pull-down assay further confirmed that P6 interacts with OsTSN1 (Fig. 2e). It is noteworthy that P6 could also interact with TSNs of *N. benthamiana* and *Zea mays* in Y2H assays (Supplementary Fig. 3). To determine which amino acid (aa) residues in P6 were responsible for the interaction between P6 and OsTSN1, we first analyzed the N-P6, C-P6, C-P6a, and C-P6b fragments (Supplementary Fig. 1a) and found that only the C-P6b fragment was able to interact with OsTSN1 in the Y2H assay (Supplementary Fig. 4a). Next, we constructed different deletion mutants of OsTSN1, including N-OsTSN1, C-OsTSN1, N-OsTSN1$^{\triangle SN1}$, N-OsTSN1$^{\triangle SN2}$, N-OsTSN1$^{\triangle SN3}$, and N-OsTSN1$^{\triangle SN4}$ (Supplementary Fig. 4b). Our Y2H and BiFC assays showed that the deletion of the SN3 domain from OsTSN1 abolished its interaction with P6 (Supplementary Fig. 4c, d). Sequencing alignment analysis showed that the SN3 domain of OsTSN2 contains 25 aa residues that differ from the other analyzed TSN proteins (Supplementary Fig. 5a). We then generated OsTSN1 mutant (OsTSN1^{SN3m}) by replacing all these 25 diverse aa residues with Ala residues. Y2H assay result demonstrated that OsTSN1^{SN3m} can not interact with P6 (Supplementary Fig. 5b), suggesting that these 25 aa residues in SN3 domain play a decisive role in the TSN-P6 interaction. Using AF2 prediction with the sequences of C-P6b and OsTSN1-SN3 domain, we identified Gln (aa 42) and Tyr (aa 57) residues of P6 as the key interaction sites (Fig. 2f). To confirm this, we created one or two site-directed mutants of P6 by replacing single Gln (aa 42) or Tyr (aa 57) residues, or both, with Ala residues. The Y2H assay results showed that all three P6 mutants lost their ability to interact with OsTSN1, indicating the importance of these two aa residues in the P6-OsTSN1 interaction (Fig. 2g).

AtTSNs, the orthologs of OsTSN1, have been predicted to undergo phase separation and participate in the formation of SGs and PBs during heat stress[48]. To investigate the characteristics of OsTSN1, we analyzed the OsTSN1 sequence and discovered three IDR domains in its SN domains (Supplementary Fig. 6a). GFP-OsTSN1 expressed in *N. benthamiana* leaf cells or rice protoplasts could form droplets under heat shock or salt stress conditions, but not under normal conditions (Supplementary Fig. 6b). Furthermore, the presence of P6 also induced the formation of OsTSN1 droplets (Supplementary Fig. 6c). Additionally, FRAP assay showed that P6-induced droplets could rapidly recover after photobleaching (Supplementary Fig. 6d, e and Video.1). When co-expressed with P6 mutant (P6^{Q42A,Y57A}), OsTSN1 did not produce droplets, as when co-expressed with the GUS (Supplementary Fig. 6c). To further confirm whether the P6-OsTSN1 interaction can promote OsTSN1 to undergo LLPS and form droplets in rice, we expressed GFP-OsTSN1 in rice protoplasts isolated from wildtype (WT) rice and P6-OE transgenic and found that OsTSN1 droplets appeared in protoplasts isolated from P6-OE transgenic plants compared to the WT (Fig. 2h), these results demonstrating that the P6-OsTSN1 interaction can promote OsTSN1 to undergo LLPS and form droplets. Furthermore, purified prokaryotically expressed P6 and OsTSN1 proteins also formed colocalized droplets in vitro (Fig. 2i). Taken together, these data demonstrate that OsTSN1 acts as SRBSDV P6 interacts with OsTSN1 to form droplets.

OsTSN1 positively regulates SRBSDV infection

To investigate the effect of P6-OsTSN1 droplets on SRBSDV infection in rice, we treated rice protoplasts with 1,6-hexanediol (1,6-HD), an inhibitor that destabilizes droplets. The cell viability of protoplasts with 0.5% or 1.0% 1,6-HD treatment was not affected (Fig. 3a). Compared to untreated SRBSDV-infected rice protoplasts, transcripts of SRBSDV *P6* and *P10* in 1.0% 1,6-HD-treated SRBSDV-infected protoplasts were significantly decreased (Fig. 3b). We also found that there was no OsTSN1 droplet in uninfected protoplasts (Fig. 3c). However, the droplets formed in SRBSDV-infected protoplasts were disappeared under 1% 1,6-HD treatment (Fig. 3c). These findings above indicate that SRBSDV infection induces the OsTSN1 droplet formation, which facilitates virus infection. Next, to further determine the role of OsTSN1 in SRBSDV infection in rice, we analyzed the *OsTSN1* transcript accumulation in SRBSDV-infected plants through RT-qPCR and western blot. The results showed that, compared to uninfected rice plants, the *OsTSN1* transcript and protein accumulations were not significantly altered by SRBSDV infection (Supplementary Fig. 7a, b). We then generated two independent *OsTSN1* knockout rice lines (ostsn1#2 and ostsn1#3) using CRISPR/Cas9 technology (Fig. 3d, e). Compared to WT rice plants, the growth of the two mutant lines did not change significantly, and no obvious developmental phenotypes were observed (Fig. 3f, g). When the two knockout mutant lines and the WT rice seedlings were inoculated with SRBSDV via viruliferous *Sogatella furcifera* transmission, the SRBSDV-infected ostsn1-#2 and ostsn1-#3 mutant plants showed milder dwarfing symptoms than the SRBSDV-infected WT plants (Fig. 3f, g). The SRBSDV infection rates of mutant and WT rice plants showed no significant difference (Supplementary Data 2). RT-qPCR and western blot assays showed that the levels of SRBSDV *P10* gene and protein were significantly reduced in the infected ostsn1#2 and ostsn1#3 mutant plants compared to those in the WT plants (Fig. 3h, i). These findings indicate that OsTSN1 positively regulates SRBSDV infection. To further test this notion, we generated two OsTSN1 overexpression transgenic lines (OsTSN1-OE#5 and OsTSN1-OE#7) (Fig. 3e), and inoculated them with SRBSDV as described above. By 4 weeks post inoculation, both OsTSN1-OE#5 and OsTSN1-OE#7 plants showed stronger dwarfing symptoms compared to the WT plants infected with SRBSDV (Fig. 3f, j). The infection rate of SRBSDV in OsTSN1-OE transgenic lines was higher than that in WT plants (Supplementary Data 2). Analysis of these inoculated plants showed that the levels of SRBSDV *P10* RNA and protein were significantly higher in the infected OsTSN1-OE#5 and OsTSN1-OE#7 plants than in the WT plants (Fig. 3k, l). This strongly indicates that OsTSN1 positively regulates SRBSDV infection.

SRBSDV P6 can localize in SGs via its interaction with OsTSN1

It has been reported that virus-encoded RNA silencing suppressors can accumulate in membraneless condensates[30]. To explore the relationship between P6- or P6-OsTSN1-formed droplets and membraneless condensates in cytoplasm, we constructed two plasmids expressing NbG3BP-mCherry and NbDCP1-CFP, respectively, to mark SGs and PBs. Co-expression of NbG3BP-mCherry, NbDCP1-CFP and GFP-P6 or NbG3BP-mCherry, NbDCP1-CFP, GFP-OsTSN1 and P6 in *N. benthamiana* leaf cells through agroinfiltration showed that P6-formed droplets were primarily localized within SGs (62.6%) and partially colocalized with PBs (22.9%) (Fig. 4a, b). Similarly, P6-OsTSN1-formed droplets were mainly localized in SGs (64.9%) with a smaller fraction in PBs (24.2%) (Fig. 4a, b). Notably, the overlapping regions of P6-formed

https://doi.org/10.1038/s41467-025-62395-5

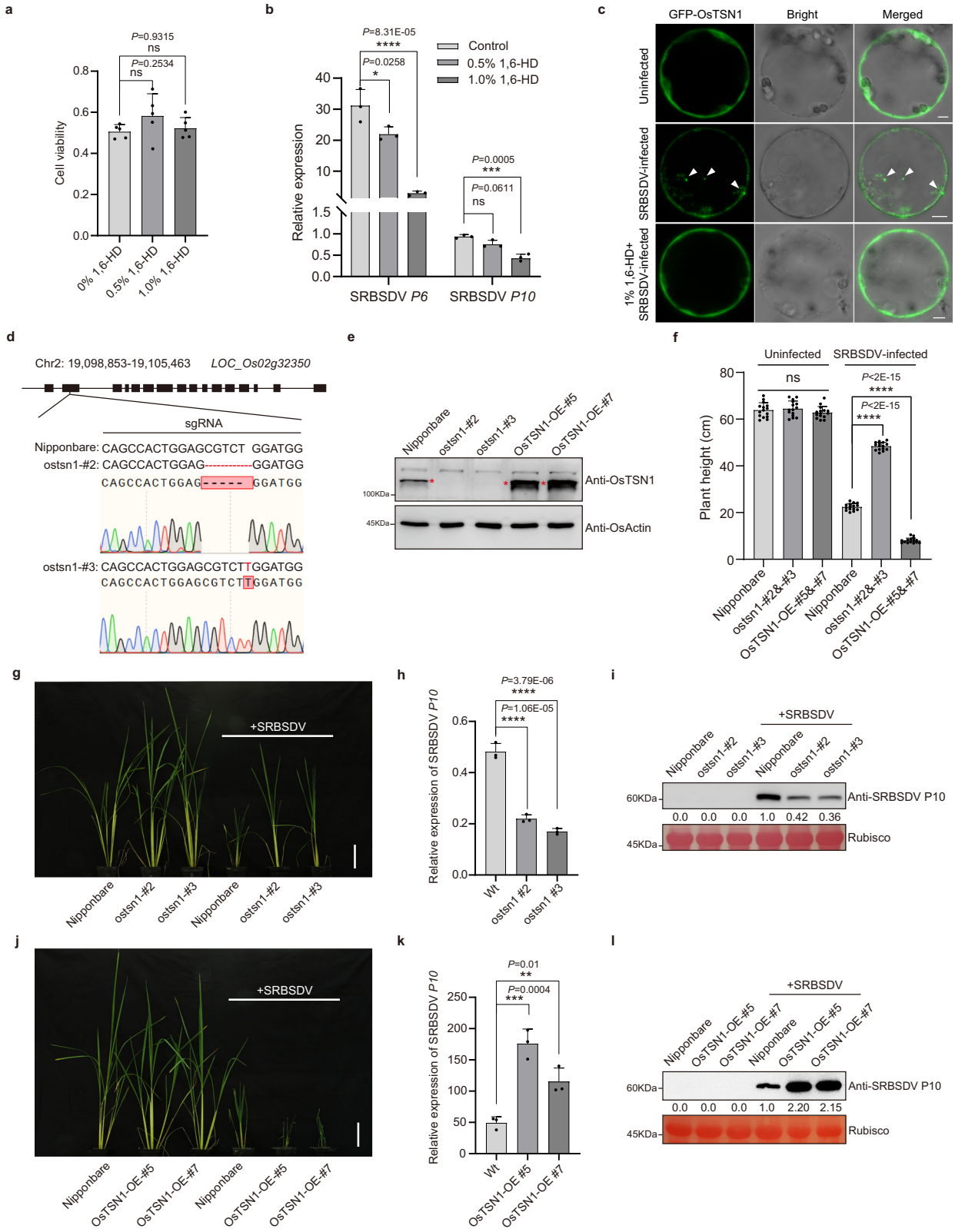

droplet-PB and P6-OsTSN1-formed droplet-PB co-localization granules were also localized to SGs (Fig. 4a).

Next, we investigated whether the formation of P6-associated SGs required the involvement of TSN proteins. We constructed a TRV-based VIGS vector to simultaneously silence the expression of all three *NbTSN* members (i.e., Niben101Scf02027g01022.1, Niben101Scf02581g03002.1, and Niben101Scf07579g04003.1) in *N. benthamiana* plants through agroinfiltration. Compared to the plants infected with TRV-*GUS*, the phenotype of plants infected with TRV-*NbTSN* was not obviously affected (Supplementary Fig. 8a). The results of RT-qPCR showed that by 8 dpi, *NbTSN*s in the TRV-*NbTSN*-inoculated plants were significantly silenced (Supplementary Fig. 8b). We then transiently co-expressed mCherry-NbG3BP with GFP-P6, GFP-P6 and flag-NbTSN1, or GFP-P6 and flag-OsTSN1 in the *NbTSN*-silenced or non-

Fig. 3 | OsTSN1 negatively regulates rice antiviral defense responses. a Cell viability of rice protoplasts under 1,6-HD treatments. Data are the means ± SD from five independent biological replicates, determined using one-way ANOVA with Tukey's test. ns, no significant statistical difference. **b** RT-qPCR showing the expression levels of SRBSDV *P6* and *P10* genes in SRBSDV-infected rice protoplasts treated with 0%, 0.5% and 1% 1,6-HD. Data are the means ± SD from three independent biological replicates, determined using one-way ANOVA with Tukey's test. ns, no significant statistical difference, $^{*}P < 0.05$, $^{***}P < 0.001$, $^{****}P < 0.0001$. **c** Subcellular localization of OsTSN1 in uninfected, SRBSDV-infected rice protoplasts and SRBSDV-infected rice protoplasts with 1% 1,6-HD treatment. White arrows indicate droplets. Scale bar, 5 μm. **d** Gene sequencing results showing a 5 bp deletion or one T insertion in ostsn1#2 and ostsn1#3 knockout mutant rice lines, respectively. **e** Western blot showing the expression levels of OsTSN1 in WT, two ostsn1 knockout mutant lines, and two OsTSN1-OE transgenic rice lines. The expression level of OsActin was used as normalizer. **f** Heights of uninfected and SRBSDV-infected WT, ostsn1 knockout mutant and OsTSN1-OE transgenic rice plants. Data are the means ± SD ($n = 15$) from three independent biological experiments, determined using one-way ANOVA with Tukey's test. ns, no significant statistical difference, $^{****}P < 0.0001$. **g**–**l** Phenotypes and virus accumulations of SRBSDV-infected WT, ostsn1 knockout mutant and OsTSN1-OE transgenic rice plants. Phenotypes of uninfected or SRBSDV-infected WT, ostsn1 knockout mutant rice (**g**) and OsTSN1-OE transgenic plants (**j**) at 30 dpi. Scale bar, 10 cm. RT-qPCR showing the expression level of SRBSDV *P10* gene in SRBSDV-infected WT, ostsn1 knockout mutant (**h**) and OsTSN1-OE transgenic plants (**k**) at 30 dpi. Data are the means ± SD from three independent biological replicates per treatment, determined using one-way ANOVA with Tukey's test. $^{****}P < 0.0001$. Western blot assay showing the accumulation of SRBSDV P10 in SRBSDV-infected WT, ostsn1 knockout mutant (**i**) and OsTSN1-OE transgenic plants (**l**) at 30 dpi. The Rubisco bands are used to show equal loading. Experiments in (**c**, **e**, **i**, and **l**) were repeated three times with similar results.

silenced *N. benthamiana* leaves. To induce more SGs for confocal microscope observation, we also treated *N. benthamiana* leaves with 42 °C heat shock. The results showed that more SGs were occurred under heat shock (Supplementary Fig. 9a). Moreover, after silencing *NbTSNs*, few SGs were found in the cells and thus, there was almost no co-localization with the GFP-P6-formed droplets (Fig. 4c and Supplementary Fig. 9b). As expected, in the non-silenced control plants, many SGs were found in the cells and were colocalized with the GFP-P6-formed droplets (Fig. 4c and Supplementary Fig. 9b). Additionally, when NbTSN1 or OsTSN1 were co-expressed with GFP-P6 in *NbTSN*-silenced *N. benthamiana* leaf cells, most SGs colocalized with the GFP-P6-formed droplets (Fig. 4c and Supplementary Fig. 9b). Quantitative statistical analysis of colocalized GFP-P6-SG droplets in different leaf samples confirmed these observations (Fig. 4d). We further isolated SGs from agroinfiltrated *N. benthamiana* leaves through differential centrifugation[56] and examined them under a confocal microscope (Fig. 4e). Western blot assay corroborated that GFP-P6 was indeed present in the SGs isolated from the TSN1-expressing *N. benthamiana* leaves (Fig. 4f).

LLPS driven by P6 enhances the nuclease activity of OsTSN1 through facilitating its multimerization

TSN1 exhibits the capacity for self-interaction, leading to the formation of homodimers[46]. To explore the relationship between nuclease activity of OsTSN1 and its self-interaction properties, we synthesized *GFP* single-stranded RNA (ssRNA) and double-stranded RNA (dsRNA) and extracted SRBSDV genomic RNA from SRBSDV-infected rice plants using the cellulose extraction method. The resulting RNAs were incubated with purified His-OsTSN1 followed by an RNA degradation assay. The results showed that OsTSN1 can degrade *GFP* ssRNA, but not *GFP* dsRNA or SRBSDV gRNA (Supplementary Fig. 10a–c). We then tested the nuclease activity of OsTSN1 and its six truncated mutants (i.e., N-OsTSN1, C-OsTSN1, N-OsTSN1$^{\triangle SN1}$, N-OsTSN1$^{\triangle SN2}$, N-OsTSN1$^{\triangle SN3}$, N-OsTSN1$^{\triangle SN4}$) on *GFP* ssRNA, and discovered that only N-OsTSN1, the N-terminal half of OsTSN1, has nuclease activity, and all SN1-4 mutants can affect the nuclease activity of OsTSN1 (Supplementary Fig. 10d, e). Using the BiFC assay, we confirmed that OsTSN1 is capable of self-interacting to form dimers (Supplementary Fig. 11a). Next, we cross-linked the purified prokaryotically expressed MBP-OsTSN1 using various concentrations of glutaraldehyde. The results showed that cross-linking with 0.01% or 0.1% glutaraldehyde caused the formation of MBP-OsTSN1 dimers and multimers, but not for the MBP-tag alone (Supplementary Fig. 11b). To further validate the formation of OsTSN1 multimer, we performed size-exclusion chromatography coupled with high-performance liquid chromatography (SEC-HPLC) assay. The results showed that the purified His-OsTSN1 recombinant protein spontaneously formed two distinct multimeric peaks separately with a minor high-molecular-weight (>669 kDa) multimer and a major low-molecular-weight (450 kDa–669 kDa) multimer (Supplementary Fig. 11c, d). Treatment with 0.01% and 0.05% glutaraldehyde significantly enhanced the peak of the high-molecular-weight multimer (Supplementary Fig. 11d), indicating that the glutaraldehyde cross-linking promotes OsTSN1 multimerization. Then, we treated purified His-OsTSN1 with different concentration of DTT prior to SDS-PAGE, and the electrophoresis result showed that compared with 1 mM DTT treatment, DTT concentrations ranging from 10 mM to 500 mM induced the dissociation of OsTSN1 multimers (Supplementary Fig. 11e). Furthermore, SEC-HPLC analysis confirmed that 10 mM and 100 mM DTT treatments resulted in the decrease or even disappearance of two multimeric peaks of OsTSN1 (Supplementary Fig. 11f), indicating that high concentration DTT treatment causes disassembly of TSN1 multimers. Collectively, the above findings demonstrated that OsTSN1 has the capacity to form multimers.

To investigate the effect of multimerization of OsTSN1 on its nuclease activity, we performed a nuclease activity assay using purified His-OsTSN1 and different concentrations of glutaraldehyde. The results showed that the nuclease activity of OsTSN1 was enhanced at concentrations of 0.001% or 0.01% glutaraldehyde (Supplementary Fig. 11g). However, when the concentrations of glutaraldehyde reached 0.05% or higher, the nuclease activity was inhibited. Furthermore, we found that the nuclease activity of OsTSN treated with high concentration DTT (ranging from 10 mM to 500 mM) was significantly decreased (Supplementary Fig. 11h). These findings indicate that the effect of OsTSN1 nuclease activity depends on its multimerization. As P6 can interact with OsTSN1 and form droplets localized at SGs, we decided to test the effect of LLPS driven by P6 on the multimerization and nuclease activity of OsTSN1 in plant cells. nYFP-OsTSN1, OsTSN1-cYFP and mCherry-OsTSN1 were co-expressed with different concentrations of P6 in *N. benthamiana* leaves through agroinfiltration. Under the confocal observation, the size of OsTSN1-formed droplets gradually enlarged with increasing P6 protein concentration (Fig. 5a, b). To validate this finding, a competitive pull-down assay was carried out in vitro, and the result showed that the amount of pulled down His-OsTSN1 gradually increased with increasing P6 amount (Fig. 5c). Moreover, SEC-HPLC analysis further revealed that P6 enhanced the formation of OsTSN1 multimer in vitro (Fig. 5d). We then extracted total protein from uninfected, SRBSDV-infected and P6-OE transgenic rice plants using a non-denaturing method[56]. Western blot results showed that, compared to the uninfected plants, an additional OsTSN1 multimer band was observed in SRBSDV-infected and P6-OE transgenic rice plants (Fig. 5e). Furthermore, we obtained OsTSN1 through Co-IP using an OsTSN1 antibody and found that nuclease activity of OsTSN1 in SRBSDV-infected and P6-OE transgenic plants was significantly increased compared to that in uninfected plants (Fig. 5f). Next, we examined the effect of 1,6-HD on the nuclease activity of OsTSN1. The growth phenotype of rice seedings treated with 1,6-HD for 12 h showed no significant changes compared with untreated control (Supplementary Fig. 12). Compared with the untreated control, the nuclease activity

https://doi.org/10.1038/s41467-025-62395-5

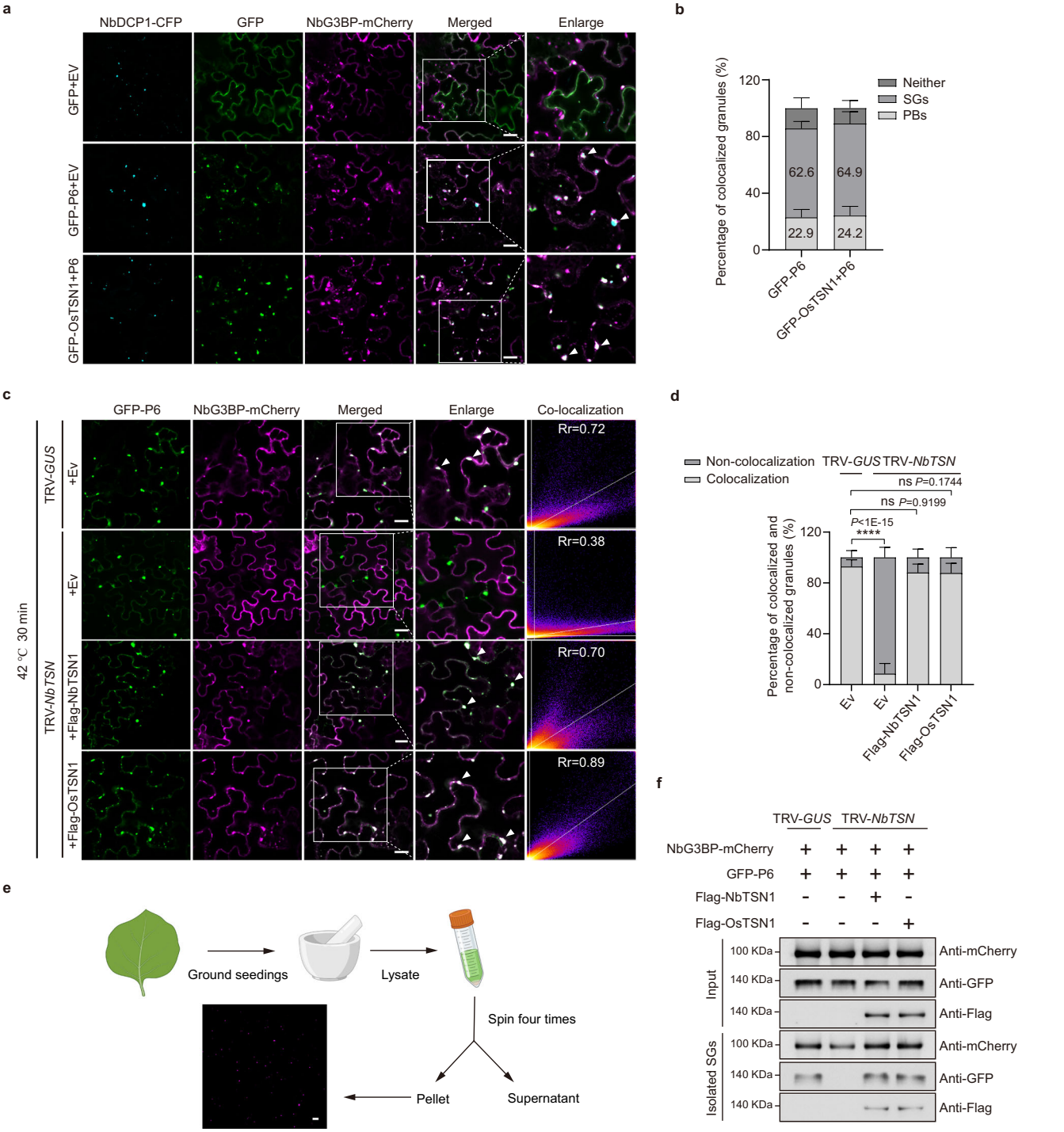

Fig. 4 | SRBSDV P6 co-localizes with SGs via its interaction with OsTSN1. **a** Subcellular co-localization of P6, PBs, and SGs in the agroinfiltrated *N. benthamiana* leaf cells at 2 days post agroinfiltration (dpa). The expressed NbDCP1-CFP and NbG3BP-mCherry were used as a PB marker and an SG marker, respectively. Scale bar, 20 μm. **b** Percentage of P6 or P6-OsTSN1 droplets colocalized with PBs and SGs in (**a**). Error bars represent SD, values are means ± SD ($n = 12$) from three independent biological experiments. **c** Subcellular co-localization of P6 and SGs in TRV-*GUS*- or TRV-*NbTSN*- inoculated *N. benthamiana* leaf cells, or in the TRV-*NbTSN*- inoculated *N. benthamiana* leaf cells expressing flag-NbTSN1 or flag-OsTSN1. NbG3BP-mCherry was used as an SG marker. In this experiment, we co-expressed GFP-P6 and NbG3BP-mCherry, GFP-P6, NbG3BP-mCherry and flag-NbTSN1, and GFP-P6, NbG3BP-mCherry and flag-OsTSN1 in leaves of *N. benthamiana* plants at 8 d post TRV-*GUS* or TRV-*NbTSN* inoculation. Two days post co-inoculation, the *N. benthamiana* plants were heated at 42 °C for 30 min followed by confocal microscopy observation. The resulting data were analyzed using the Coloc2 of ImageJ software (1.53 v). Rr represents the Pearson Coefficiency. Scale bar, 20 μm. **d** The percentage of colocalized and non-colocalized granules of P6 and SGs in different assayed leaves in (**c**). Values are means ± SD ($n = 12$) from three independent biological experiments, determined using the one-way ANOVA with Tukey's test. ns, no significant statistical difference, $^{****}P < 0.0001$. **e** A schematic diagram showing the procedure of SG isolation from *N. benthamiana* leaves and the isolated SGs. Fluorescence signal from the isolated SGs marked by NbG3BP-mCherry was captured under a confocal microscope. Scale bar, 10 μm. The schematic diagram was created in BioRender. Zeng, M. (2025) https://BioRender.com/dqw0hn8. **f** Western blot results showing the accumulation of P6 in isolated SGs from various samples described in (**c**). Experiments in (**a**, **c**, and **f**) were repeated three times with similar results.

https://doi.org/10.1038/s41467-025-62395-5

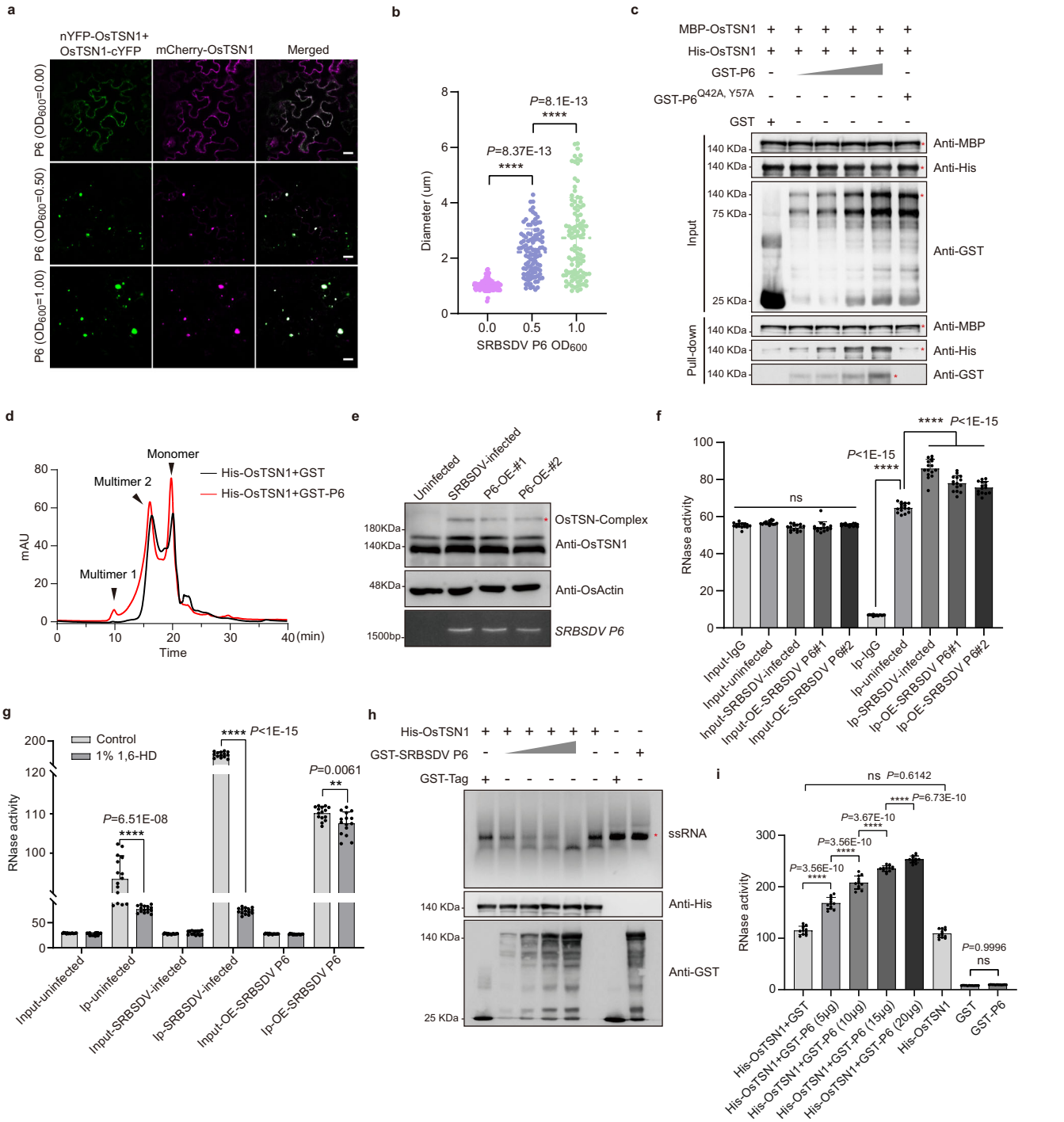

of OsTSN1 was obviously decreased in 1,6-HD-treated rice plants (Fig. 5g). Analogously, in SRBSDV-infected rice and P6-OE transgenic plants, the nuclease activity of OsTSN1 were also declined under 1,6-HD treatment conditions (Fig. 5g). Finally, we analyzed the in vitro nuclease activity of His-OsTSN1 after addition of different amounts of GST-P6. The results showed that as the amount of GST-P6 increased, the in vitro nuclease activity of His-OsTSN1 also increased (Fig. 5h, i). Based on these findings, we conclude that LLPS driven by P6 can enhance the nuclease activity of OsTSN1 by promoting its multimerization.

P6 promotes the OsTSN1-mediated degradation of host mRNAs in SRBSDV-infected rice plants

Given that OsTSN1 is an RBP, we hypothesize that P6 could promote OsTSN1 to degrade its targeted RNAs through accelerating the multimerization of OsTSN1 in P6-OsTSN1 droplets in SGs. To test this hypothesis, we prepared an anti-OsTSN1 polyclonal antibody and performed a cross-linking RNA immunoprecipitation (CLIP) assay using extracts from SRBSDV-infected and uninfected rice plants, followed by high-throughput nucleic acid sequencing (CLIP-seq) to identify the OsTSN1-targeted host RNAs. Through this analysis, a total of 1393 OsTSN1-interacting mRNAs were common in both uninfected and SRBSDV-infected samples. Additionally, specific 1,966 and 1,237 mRNAs were separately found in OsTSN1 complexes from uninfected and SRBSDV-infected plants (Supplementary Fig. 13a). OsTSN1 is mainly bound with the coding regions of these target mRNAs (Supplementary Fig. 13b, c). However, the exceptionally low mapping ratio (0.01% and 0.07%) of SRBSDV transcripts in OsTSN1-targeted RNAs suggested that P6-OsTSN1 can not effectively recruit SRBSDV

Fig. 5 | SRBSDV P6 enhances OsTSN1 nuclease activity via promoting its multimerization. a Confocal microscope showing SRBSDV P6 promotes OsTSN1 multimerization in *N. benthamiana* leaf cells at 2 dpa. Scale bar, 20 μm. **b** Statistical analysis of the diameter size of P6-OsTSN1 droplets shown in **a** ($n = 101$, 104, 102 droplets, respectively), using the ImageJ software (1.53 v). The data are the means ± SD from three independent biological experiments, determined using the one-way ANOVA with Tukey's test. $^{****}P < 0.0001$. **c** SRBSDV P6 promotes OsTSN1 multimerization in vitro. In this competitive binding pull-down assay, His-OsTSN1 was pulled down in the presence of different concentrations of GST-P6, by MBP-OsTSN1 or MBP-coupled sepharose beads. GST and GST-P6^{Q42A,Y57A} were used as controls. The proteins were analyzed using anti-MBP, anti-GST, and anti-His antibodies. **d** SEC-HPLC profile of OsTSN1 multimers triggered by GST-P6 in vitro. The peaks of the monomer and multimers were indicated by black arrows. **e** Western blot showing the OsTSN1-formed multimers in uninfected, SRBSDV-infected, and P6-OE transgenic rice plant cells using an anti-OsTSN1 antibody. The expression level of OsActin protein was used to show equal loading. The mRNA accumulation of SRBSDV *P6* was determined through RT-PCR. **f**, **g** OsTSN1 nuclease activity in uninfected, SRBSDV-infected, and P6-OE transgenic rice plants (**f**), and in 1% 1,6-HD-treated rice plants, SRBSDV-infected rice plants and P6-OE transgenic rice plants (**g**). Non-treated rice plants were used as controls. OsTSN1 monomer and multimers in rice were co-immunoprecipitated by anti-OsTSN1 antibodies. Values are the means ± SD ($n = 15$) from three independent biological experiments, determined using the one-way ANOVA with Tukey's test. ns, no significant statistical difference, $^{**}P < 0.01$, $^{****}P < 0.0001$. **h** In vitro assay result showing the P6-regulated OsTSN1 nuclease activity. GST was used as a control. The ssRNA degradation was determined by nucleic acid electrophoresis. **i** In vitro fluorometric assay showing the P6-regulated OsTSN1 nuclease activity. Values are the means ± SD ($n = 12$) from three independent experiments, determined using the one-way ANOVA with Tukey's test. ns, no significant statistical difference, $^{****}P < 0.0001$. Experiments in (**a**, **c**, **e**, and **h**) were repeated three times with similar results.

transcripts (Supplementary Data 3). According to the results of Hypergeometric Optimization of Motif EnRichment (HOMER) analysis, we hypothesized that the G-A-rich motif (GAGGAG) in the transcripts is likely the primary binding site of OsTSN1 (Supplementary Data 4), which also exists in the *GFP* ssRNA. To validate this hypothesis, we performed EMSA and RNA pull-down assays, showing that OsTSN1 is bound to transcripts with the GAGGAG motif (Fig. 6a, b). Of the targeted transcripts, the abundance of 55 was significantly different between samples from uninfected and SRBSDV-infected rice plants (Supplementary Data 5). The Gene Ontology (GO) and Kyoto Encyclopedia of Genes and Genomes (KEGG) analysis revealed that the 55 targeted mRNAs of OsTSN1 were enriched in terms related to transcriptional regulation, stress response, and metabolic pathways (Supplementary Fig. 13d). To clarify the transcript abundance of these 55 targeted mRNAs in healthy, infested, SRBSDV-infected, and P6-OE transgenic rice plants, we performed RNA-seq. Our RNA-seq data showed that nine targeted transcripts were significantly decreased in both P6-OE transgenic and SRBSDV-infected plants compared with healthy or infested plants (Supplementary Fig. 14a, b). Moreover, combined with our CLIP-seq data, only six transcripts of NAC family transcription factors (NAC15, NAC75, NAC90), transcription factor HBP-1b (TGA6), MYB family transcription factor (LHY) and bZIP transcription factor domain containing protein (bZIP23-like), were strongly targeted by OsTSN1 in SRBSDV-infected rice plants (Fig. 6c and Supplementary Fig. 15), suggesting that they are likely degraded by OsTSN1. The binding between these six mRNAs and OsTSN1 was further validated through CLIP-qPCR, and the enrichment rates (IP/Input) of these six mRNAs were significantly increased in both SRBSDV-infected rice plants and P6-OE transgenic rice plants (Fig. 6d and Supplementary Fig. 16). Next, we further analyzed the accumulation of these transcripts in WT, SRBSDV-infected, P6-OE transgenic, and ostsn1 knockout mutant rice plants and found that their transcript levels were significantly reduced in SRBSDV-infected and P6-OE transgenic plants compared to those in WT plants (Supplementary Fig. 17a, b), whereas their transcript levels in the ostsn1 knockout mutant plants were significantly up-regulated (Supplementary Fig. 17c).

To explore the function of OsNAC90, OsNAC15, OsNAC75, OsTGA6, OsLHY and OsbZIP23-like in SRBSDV infection, we generated individual knockout mutant rice plants of these genes (i.e., osnac90, osnac15, osnac75, ostga6, oslhy, and osbzip23-like) (Supplementary Fig. 18) and then inoculated them with SRBSDV through *S. furcifera* transmission. SRBSDV-infected osnac75, osbzip23 and osnac90 knockout mutant rice plants showed similar symptoms and virus accumulation as WT plants (Supplementary Fig. 19, 20). However, SRBSDV-infected osnac15, oslhy, and ostga6 mutant plants showed more severe dwarfing symptoms than WT plants (Fig. 6e–g and Supplementary Fig. 20). Results of RT-qPCR and western blot assays showed that RNA and protein levels of SRBSDV P10 were significantly increased in osnac15, oslhy, and ostga6 knockout mutant plants compared to WT plants (Fig. 6h–m), suggesting that these three genes negatively regulate SRBSDV infection and their transcripts are degraded by OsTSN1 in the presence of the virus.

OsNAC15 regulates the transcription of *OsATG8C*, while OsLHY regulates the transcription of OsJAZs

The more severe disease symptoms and higher virus accumulation in the osnac15 and oslhy knockout mutant plants prompted us to further investigate the roles of *OsNAC15* and *OsLHY* in SRBSDV infection. To investigate the transcriptional activity of OsLHY and OsNAC15, we performed a Y1H assay. The results displayed that the yeast cells co-transformed with the pGBKT7 and pGADT7-OsNAC15 vectors could grow on the SD-Trp-Leu-His-Ade medium, whereas the cells co-transformed with the pGBKT7 and pGADT7-OsLHY could not (Supplementary Fig. 21a). The dual-luciferase assay results further showed that co-expression of pBD-OsNAC15 and the reporter in *N. benthamiana* leaves significantly enhanced the luminescence intensity and the firefly luciferase/Renilla luciferase (LUC/REN) ratio, similar to the positive control, which was the co-expression of pBD-VP16 and the reporter (Supplementary Fig. 21b–d). On the other hand, co-expression of pBD-OsLHY and the reporter in *N. benthamiana* leaves significantly decreased the luminescence intensity and the LUC/REN ratio compared to the negative control, which was the co-expression of pBD empty and the reporter (Supplementary Fig. 21b, e, f). These results indicate that OsNAC15 is a transcription activator, while OsLHY is a transcription repressor.

We searched the PlantRegMap and RiceTFtarget Database[57,58], and identified 740 potential OsLHY-targeted genes with the binding motif AAGATATTT (Supplementary Data 6). OsLHY, predicted to function as an MYB-related transcriptional repressor, is thought to interact with the binding motif AAGATATTT[59]. The Y1H assay results showed that the yeast cells co-transformed with pHis-3xAAGATATTT (the main motif targeted by OsLHY) and pGADT7-OsLHY grew on the SD-Trp-Leu-His medium supplemented with 150 mM 3-AT (Supplementary Fig. 22a). The electrophoretic mobility shift assay (EMSA) result also demonstrated that OsLHY could bind to the biotin-labeled probe with an AAGATATTT motif, and the unlabeled probe with AAGATATTT motif could interfere with the binding between OsLHY and the labeled probe. As expected, the AT-rich motif mutant probe did not affect the binding between OsLHY and the labeled probe (Fig. 7a). Meanwhile, we discovered 447 OsNAC15-targeted genes without a specific binding motif by searching the PlantRegMap and RiceTFtarget Database (Supplementary Data 7). To identify the potential target motifs of OsNAC15, we performed a transcription factor-centered yeast-one-hybrid (TF-centered Y1H) assay as described previously[60]. The results of the assay using the SD-Trp-Leu-His medium supplemented with 100 mM 3-AT showed that OsNAC15 had 13 potential binding motifs (Supplementary Data 8). Then, Y1H and EMSA assays were further carried out, demonstrating that OsNAC15 can bind to the motif AGCAAGA (Fig. 7b and Supplementary Fig. 22b).

https://doi.org/10.1038/s41467-025-62395-5

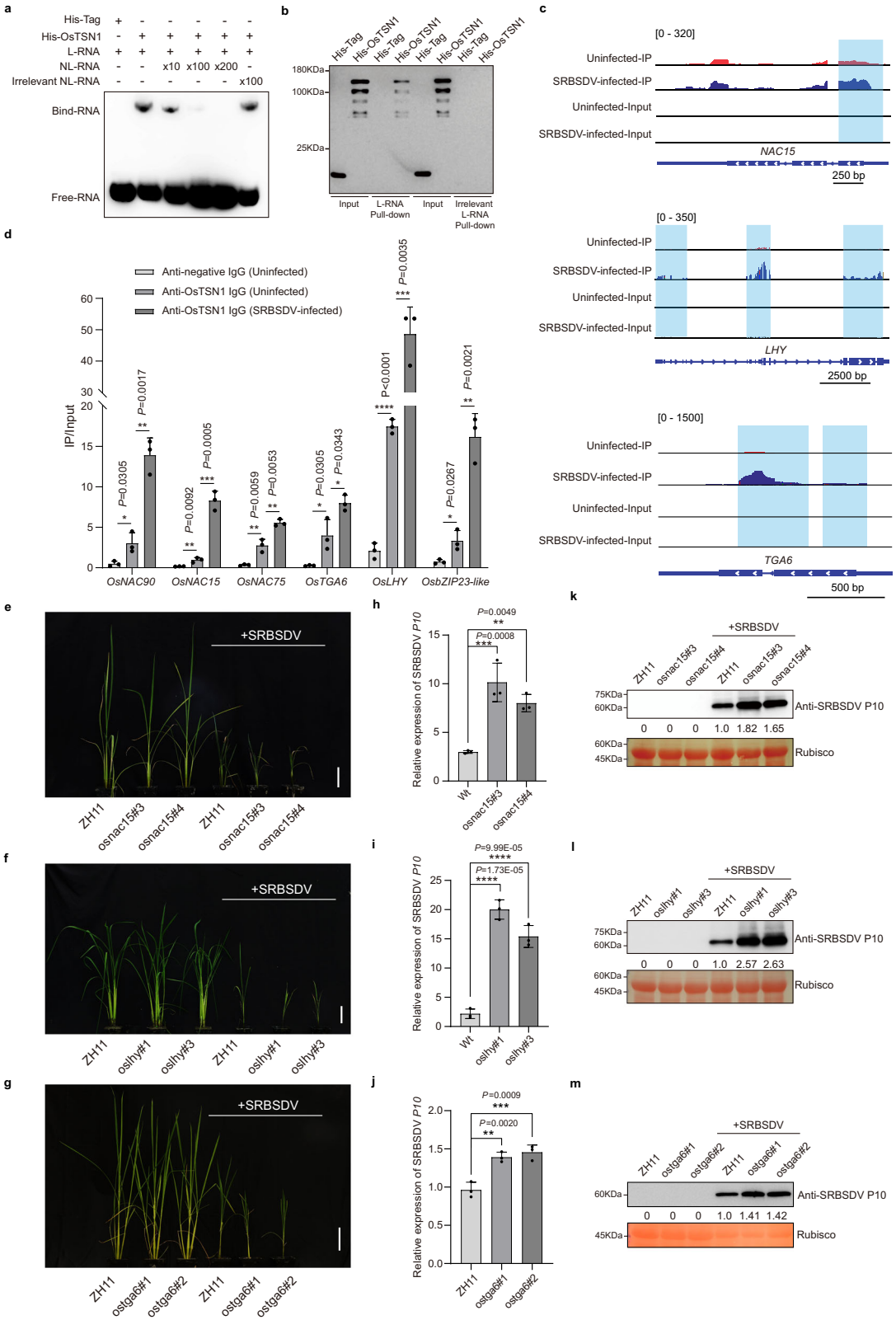

Given that OsLHY and OsNAC15 negatively regulate SRBSDV infection in rice, we focused on putative potential target genes involved in plant immune response. Among them, *jasmonate ZIM-domain 6, 12, 15* (*JAZ6, JAZ12, JAZ15*) and *autophagy-related protein 8 C* (*ATG8C*) drew our attention. It is noteworthy that a unique binding motif was found in the promoter regions of these genes using the MEME-FIMO tool (https://meme-suite.org/meme/tools/fimo) (Fig. 7c). We performed Y1H assays and found that OsLHY can bind promoter regions of *OsJAZ6*, *OsJAZ12*, *OsJAZ15* with the AAGATATTT motif, and OsNAC15 can bind the promoter region of *OsATG8C* with the AGCAAGA motif (Fig. 7d, e). Then, the whole promoter regions were cloned individually into a luciferase reporter vector (Fig. 7f) and co-expressed separately with the vector expressing OsLHY or OsNAC15 in *N. benthamiana* leaves. The intensity of luminescence and the LUC/

Fig. 6 | OsTSN1-targeted genes and their functions in SRBSDV infection. a EMSA assay result showing the in vitro binding between the purified recombinant His-OsTSN1 and the GAGGAG motif. An RNA oligo containing three-repeated 5′-GAG-GAG-3′ motifs was used as an RNA probe. L-RNA, a biotin-labeled RNA probe; NL-RNA, an unlabeled RNA probe; Irrelevant NL-RNA, a reversed unlabeled RNA probe. **b** RNA pull-down assay showing the binding between His-OsTSN1 and L-RNA or NL-RNA. His-OsTSN1 was detected using an anti-His antibody. His-tag was used as a control. **c** Integrative Genomics Viewer (IGV) graphs showing the distribution of the CLIP-seq-derived reads along *OsNAC15*, *OsLHY* and *OsTGA6* in uninfected and SRBSDV-infected rice plants. Blue boxes indicate the change regions of read distributions between uninfected and SRBSDV-infected rice plants. **d** CLIP-RT-qPCR results showing the expression levels of OsTSN1-bound *OsNAC90*, *OsNAC15*, *OsNAC75*, *OsTGA6*, *OsLHY*, and *OsbZIP23-like* transcripts. Ordinate represents the enrichment rates (IP/Input) of the immunoprecipitated RNA products from various samples, and were determined using an anti-OsTSN1 antibody. The IgG antibody was used as a control. The data are the means ± SD from three independent biological replicates, determined using two-tailed Student's *t* test. $^{*}P < 0.05$, $^{**}P < 0.01$, $^{***}P < 0.001$, $^{****}P < 0.0001$. **e**–**m** Phenotypes and virus accumulation of SRBSDV-infected WT, osnac15, oslhy and ostga6 knockout mutant rice plants at 30 dpi. Phenotypes of uninfected or SRBSDV-infected WT, osnac15, oslhy and ostga6 knockout mutant rice plants at 30 dpi (**e**–**g**). Scale bar, 10 cm. The accumulation level of SRBSDV *P10* transcripts was determined through RT-qPCR at 30 dpi (**h**–**j**). The data are the means ± SD from three independent biological replicates, determined using the one-way ANOVA with Tukey's test. $^{**}P < 0.01$, $^{***}P < 0.001$, $^{****}P < 0.0001$. The accumulation level of SRBSDV P10 protein was determined through western blot at 30 dpi (**k**–**m**). The Rubisco bands are used to show equal loading. Experiments in (**a**, **b**, **k**, **l**, and **m**) were repeated three times with similar results.

REN ratio were examined and used to determine the transcriptional level of *OsJAZ6*, *OsJA12*, *OsJA15*, and *OsATG8C*. The result showed that, compared to the empty vector control, the presence of OsLHY suppressed the expression of luciferase driven by the *OsJAZ6*, *OsJAZ12* or *OsJAZ15* promoter, whereas the presence of OsNAC15 increased the expression of luciferase driven by the *OsATG8C* promoter (Fig. 7g, h). Moreover, compared to the WT control rice plants, the expression levels of *OsJAZ6*, *OsJAZ12*, and *OsJAZ15* were markedly up-regulated in the oslhy knockout mutant rice plants, while the expression level of *OsATG8C* was significantly down-regulated in the osnac15 knockout mutant plants (Fig. 7i). Collectively, these findings indicate that OsNAC15 is a positive regulator of *OsATG8C* expression and OsLHY is a negative regulator of *OsJAZ6*, *OsJAZ12*, and *OsJAZ15* expression.

Downregulation of *OsATG8C* and *OsJAZs* expression promotes SRBSDV infection

To investigate the effect of *OsJAZ6*, *OsJAZ12*, *OsJAZ15*, and *OsATG8C* on SRBSDV infection, we generated osjaz6, osjaz12, osjaz15, and osatg8c knockout mutant rice plants. After SRBSDV inoculation, the osjaz6, osjaz12 and osjaz15 mutant plants showed milder dwarfing symptoms than the infected WT plants, while the osatg8c mutant plants showed more severe dwarfing symptoms (Fig. 8a–c and Supplementary Figs. 20 and 23a). Results of RT-qPCR and western blot assays showed that the RNA and protein accumulation levels of SRBSDV P10 were significantly lower in infected osjaz6 and osjaz12 mutant plants compared to those in infected WT plants, whereas the RNA and protein accumulation levels of SRBSDV P10 were markedly higher in infected osatg8c mutant plants (Fig. 8d–i). However, compared to the infected WT plants, both RNA and protein accumulation levels of SRBSDV P10 in the infected osjaz15 mutant plants were reduced, although this difference was not statistically significant (Supplementary Fig. 23b, c). According to the RNA-seq data from the Rice Genome Annotation Project (http://rice.uga.edu/cgi-bin/ORF_infopage.cgi), *OsJAZ15* is specifically expressed in rice anther and post-germination inflorescence, which may have less effect on SRBSDV infection. Therefore, *OsJAZ15* was not included in the subsequent experiments.

To further investigate whether OsTSN1 can regulate the transcription of *OsJAZ6*, *OsJAZ12*, and *OsATG8C* through degrading *OsLHY* and *OsNAC15* mRNAs, we purified and incubated recombinant GFP-OsTSN1 and RFP-P6 with Cy5-labeled transcripts of *OsLHY*, *OsNAC15*, or *OsUBQ5* (as a negative control) in vitro. We found that Cy5-labeled *OsLHY* and *OsNAC15* transcripts, but not Cy5-labeled *OsUBQ5* transcripts, colocalized in P6-OsTSN1 droplets (Fig. 8j). RNA degradation assays showed that OsTSN1 degraded *OsLHY* and *OsNAC15* transcripts, and this degradation was more pronounced with increasing amounts of P6 (Fig. 8k). Furthermore, the addition of the mutant GST-C-$P6^{Q42A,Y57A}$ did not affect RNA degradation (Fig. 8k). These findings indicate that the *OsLHY* and *OsNAC15* transcripts were recruited into the P6-OsTSN1 droplets and then degraded. Then, dual-luciferase assays were performed, and the results showed that, based on the LUC/REN ratio, the transcription levels of *OsJAZ6* and *OsJAZ12* were elevated in the presence of OsTSN1, whereas the transcription level of *OsATG8C* was decreased (Fig. 8l, m). In this study, we also analyzed the transcription levels of *OsJAZ6*, *OsJAZ12*, and *OsATG8C* in the ostsn1 knockout mutant, P6-OE transgenic, and OsTSN1-OE transgenic rice plants. Compared to WT plants, the transcript accumulation of *OsJAZ6* and *OsJAZ12* was significantly up-regulated in P6-OE and OsTSN1-OE transgenic rice plants, while the expression level of *OsATG8C* was significantly decreased (Supplementary Fig. 24a, b). As expected, the expression patterns of *OsJAZ6*, *OsJAZ12*, and *OsATG8C* in the ostsn1 knockout mutant plants were the opposite of those found in the P6 and OsTSN1-OE transgenic plants (Supplementary Fig. 24c). Next, we further analyzed the expression levels of *OsLHY* and *OsNAC15*, and their downstream genes *OsJAZ6*, *OsJAZ12*, and *OsATG8C* in SRBSDV-infected and uninfected rice plants at different days post inoculation. Compared to uninfected plants, the expression levels of *OsLHY*, *OsNAC15*, and *OsATG8C* in SRBSDV-infected plants were all significantly decreased at 4, 7, and 28 dpi, whereas the expression levels of *OsJAZ6* and *OsJAZ12* were significantly up-regulated (Supplementary Fig. 25). Collectively, these data suggest that P6 promotes the OsTSN1-mediated degradation of mRNAs of *OsLHY* and *OsNAC15*, potentially suppressing the JA- and autophagy-related immune response to facilitate SRBSDV infection.

Different virus-encoded RNA silencing suppressors promote multimerization and RNA decay activity of OsTSN1 for their infection

Given that SRBSDV P6 is an RNA silencing suppressor[4], we speculated that other viral RNA silencing suppressors might also be able to interact with OsTSN1 and undergo LLPS. To test this idea, we analyzed the sequences of RNA silencing suppressors from two other rice viruses, RBSDV P6 and RSV NS3[61], using PONDR and IUPred3 tools. Our prediction results showed that both suppressors have IDRs (Supplementary Fig. 26a, b), indicating that they might also have the ability to undergo LLPS. Our pull-down and BiFC assay results indicated that RBSDV P6 and RSV NS3 can interact with OsTSN1 (Supplementary Fig. 26c–f) and also form granules localized at SGs (Supplementary Fig. 26g). To test whether RBSDV P6 and RSV NS3 can promote OsTSN1 multimerization and nuclease activity, we transiently co-expressed YN-OsTSN1 and YC-OsTSN1 with four different concentrations of RBSDV P6 or RSV NS3 in *N. benthamiana* leaves. The results demonstrated that in the absence of RBSDV P6 or RSV NS3, OsTSN1 did not form droplets. However, in the presence of RBSDV P6 or RSV NS3, the size of OsTSN1 droplets gradually increased with increasing accumulation of the viral proteins (Fig. 9a–d). SEC-HPLC analysis further confirmed the formation of RBSDV P6-OsTSN1 and RSV NS3-OsTSN1 multimers (Fig. 9e). The results of the in vitro nuclease activity assay also showed that the nuclease activity of OsTSN1 was gradually enhanced as the concentration of RBSDV P6 or RSV NS3 increased (Fig. 9f, g). To elucidate the function of OsTSN1 in RBSDV and RSV infections in rice, we

https://doi.org/10.1038/s41467-025-62395-5

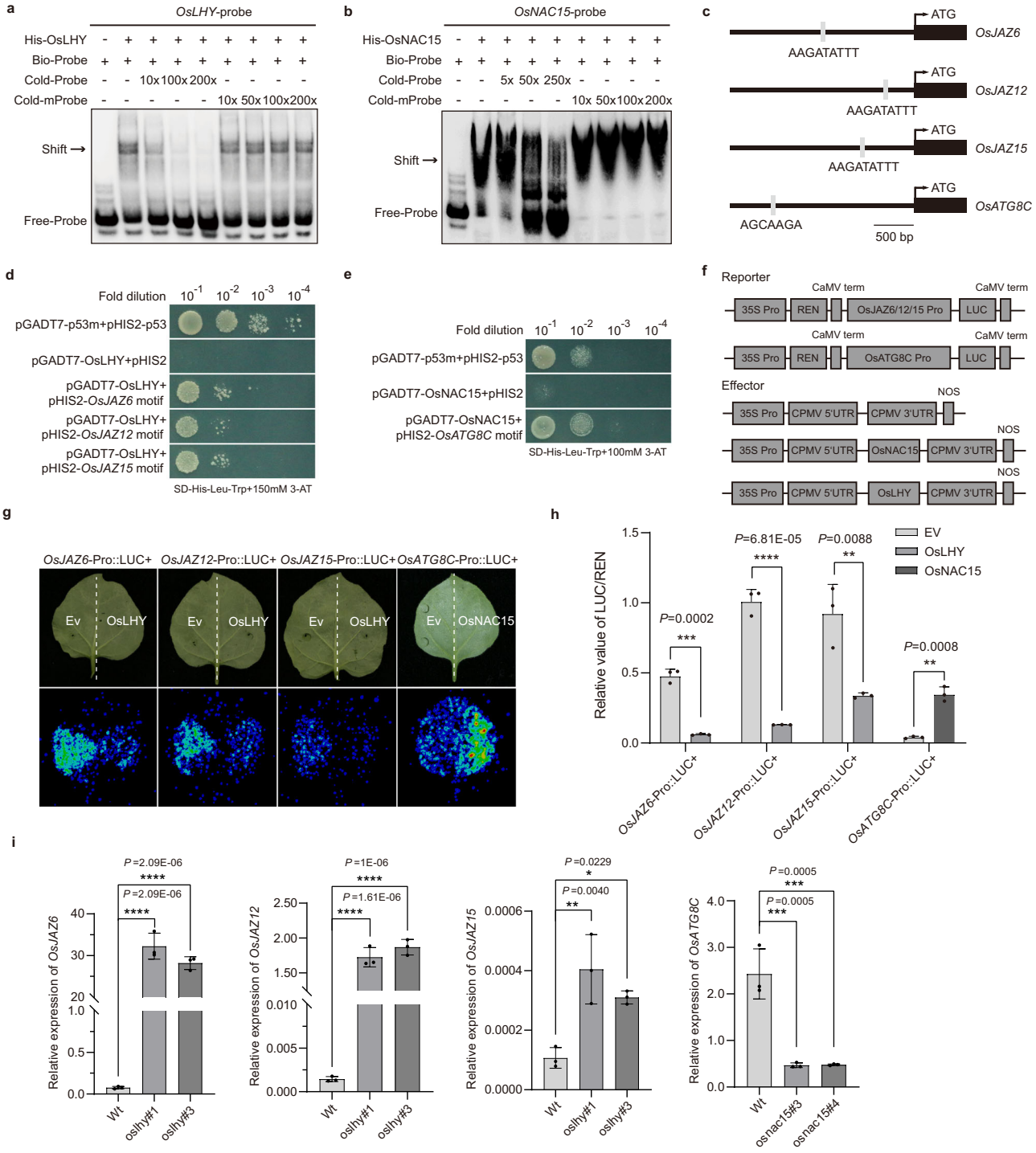

Fig. 7 | OsLHY and OsNAC15 regulate separately the transcription of *OsJAZ6, OsJAZ12, OsJAZ15* and *OsATG8C*. **a**, **b** EMSA assay showing the bonding between OsLHY (**a**) or OsNAC15 (**b**) and their probe with AAGATATTT or AGCAAGA sequences. Bio-probe is a biotin-labeled three-repeated AAGATATTT or AGCAAGA sequence. Cold probe and cold-mprobe are unlabeled three-repeated AAGATATTT or AGCAAGA sequences and their mutant sequences, respectively. **c** Analysis of the binding motif in promoters of *OsJAZ6*, *OsJAZ12*, *OsJAZ15*, and *OsATG8C*. Gray lines indicate the binding motifs. **d**, **e** Y1H assay showing the binding between OsLHY and promoter regions of *OsJAZ6*, *OsJAZ12*, and *OsJAZ15* (**d**), and OsNAC15 and promoter region of *OsATG8C* (**e**). Thirty bp sequence in promoters of *OsJAZ6*, *OsJAZ12*, *OsJAZ15* and *OsATG8C* containing AAGATATTT motif or AGCAAGA motif were amplified and cloned into pHIS2 vector. Cells co-transformed with pGADT7-p53m and pHIS2-p53 were used as a positive control. **f** The effector and reporter vectors used for the binding motif analyses in the promoter regions of the OsLHY- or OsNAC15-targeted genes. A 2000 bp region, upstream of the start codon (ATG) that contains the predicted binding motif(s), was amplified from each assayed gene and cloned into the dual-luciferase reporter vector. **g**, **h** A Dual-luciferase reporter assay showing the effects of OsLHY or OsNAC15 on transcriptions of *OsJAZ6*, *OsJAZ12*, *OsJAZ15*, and *OsATG8C* in *N. benthamiana* leaves at 2 dpa (**g**). The LUC/REN ratio was used as an indication of the transcription activity (**h**). The data are the means ± SD from three independent biological replicates, determined using a two-tailed Student's *t* test. $^{**}P < 0.01$, $^{***}P < 0.001$, $^{****}P < 0.0001$. **i** RT-qPCR showing transcriptional levels of *OsJAZ6*, *OsJAZ12*, and *OsJAZ15* in oslhy knockout mutant rice plants, and transcriptional level of *OsATG8C* in osnac15 knockout mutant rice plants. The data are the means ± SD from three independent biological replicates, determined using one-way ANOVA with Tukey's test. $^{*}P < 0.05$, $^{**}P < 0.01$, $^{***}P < 0.001$, $^{****}P < 0.0001$. Experiments in (**a**, **b**, and **g**) were repeated three times with similar results.

https://doi.org/10.1038/s41467-025-62395-5

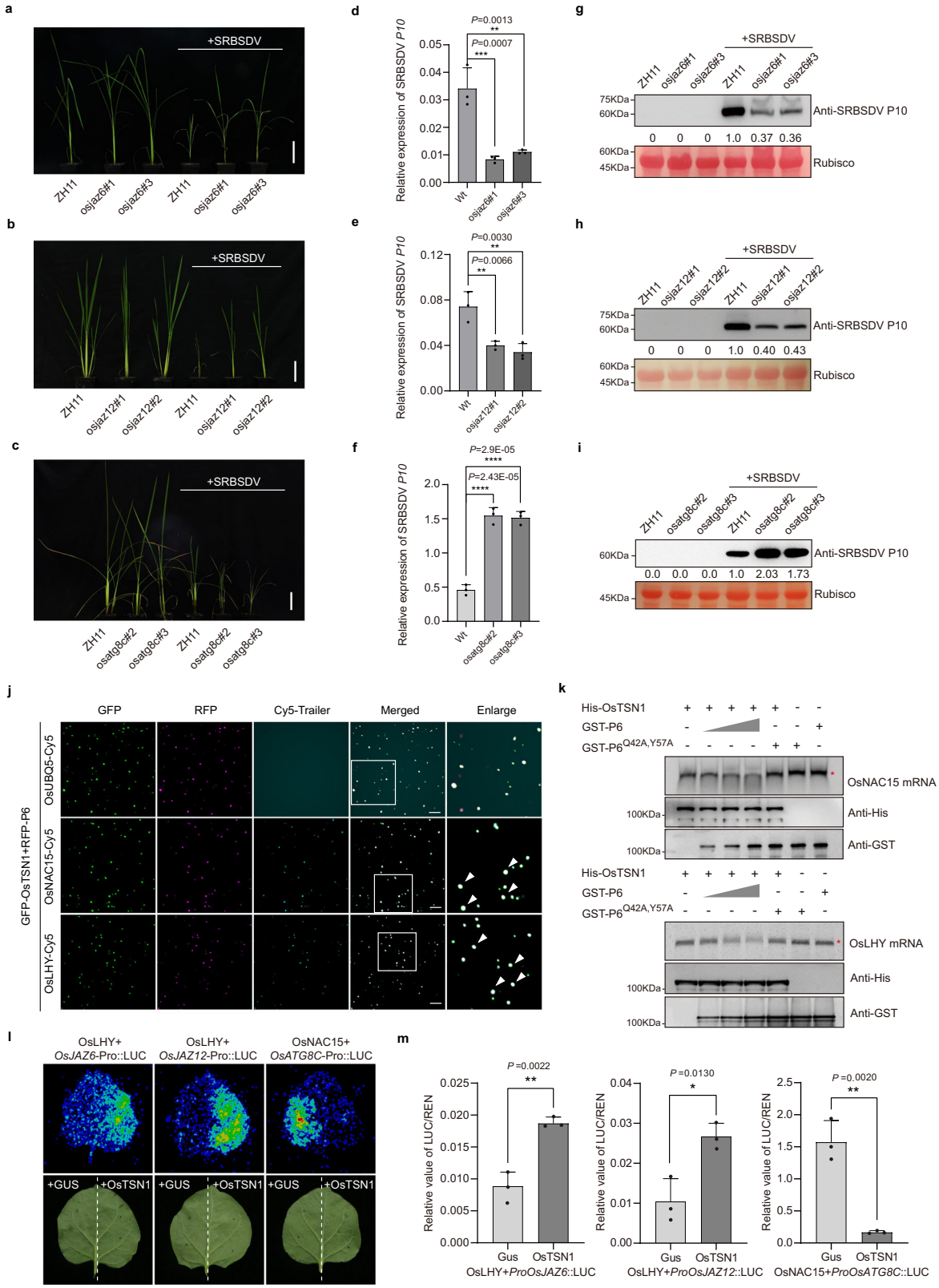

inoculated the ostsn1 knockout mutant and OsTSN1-OE transgenic rice plants with RBSDV and RSV, respectively. We discovered that, compared to WT plants, the ostsn1 knockout mutant plants showed reduced susceptibility to infection by both RBSDV and RSV (Fig. 9h–k and Supplementary Fig. 27a–e). Conversely, OsTSN1-OE transgenic plants exhibited increased susceptibility to RBSDV and RSV (Fig. 9h, l–n and Supplementary Fig. 27c, f–i). These results suggest that, in addition to SRBSDV P6, RBSDV P6, and RSV NS3 also promote OsTSN1 multimerization and cleavage activity, facilitating viral infection in rice.

Discussion

Condensates are biomolecular assemblies without surrounding membranes that are involved in various biological processes in eukaryotic cells[62,63]. They are generated via LLPS and contain specific sets of

Fig. 8 | OsTSN1 regulates the mRNA expression of *OsJAZ6*, *OsJAZ12* and *OsATG8C* via degrading the mRNAs of *OsNAC15* and *OsLHY* to promote SRBSDV infection. **a**–**i** Phenotypes of uninfected or SRBSDV-infected WT, osjaz6, osjaz12, and osatg8c knockout mutant rice plants at 30 dpi (**a**–**c**). Scale bar, 10 cm. RT-qPCR results showing the expression level of SRBSDV *P10* gene in SRBSDV-infected WT and osjaz6, osjaz12, osatg8c knockout mutant plants at 30 dpi (**d**–**f**). The data are the means ± SD from three independent biological replicates, determined using the one-way ANOVA with Tukey's test. $^{**}P < 0.01$, $^{***}P < 0.001$, $^{***}P < 0.0001$. Western blot results showing the accumulation levels of SRBSDV P10 in uninfected and SRBSDV-infected WT, osjaz6, osjaz12, and osatg8c knockout mutant rice plants (**g**–**i**). The Rubisco bands are used to show equal loading. **j** In vitro assay showing the co-localization of Cy5-labeled *OsNAC15* or *OsLHY* mRNAs with the OsTSN1-P6 droplets. *OsUBQ5* mRNA was used as a control. Scale bar, 10 μm. **k** *OsNAC15* and *OsLHY* mRNAs were degraded in vitro by recombinant OsTSN1. Different amounts of recombinant GST-P6 were incubated with recombinant OsTSN1 for 2 h before the addition of *OsNAC15* or *OsLHY* mRNAs. GST-C-P6^{Q42A,Y57A} was used as a negative control. Degradation of *OsNAC15* or *OsLHY* mRNAs was determined by nucleic acid electrophoresis. **l**, **m** OsTSN1 regulates the transcriptional levels of *OsJAZ6*, *OsJAZ12* and *OsATG8C* through degrading mRNAs of *OsLHY* and *OsNAC15*. Images were taken at 2 dpa (**l**). The LUC/REN ratio represents the relative LUC activity (**m**). The data are the means ± SD from three independent biological replicates, determined using two-tailed Student's *t* test. $^{*}P < 0.05$, $^{**}P < 0.01$. Experiments in (**g**–**l**) were repeated three times with similar results.

macromolecules[64]. In addition to normal physiological activity, membraneless condensates are also relevant to innate immunity against virus infections[65]. Conversely, viruses encode highly disordered proteins that can affect the formation of condensates via LLPS, which facilitates their replication and aids in the evasion of host antiviral defense[66–68]. However, studies on how plant viruses exploit SGs and/or PBs to benefit their infection remain limited. A recent study reported that the cauliflower mosaic virus (CaMV) can recruit PB components into viral factories to support virus replication[69]. In this study, we discovered that the silencing suppressors of SRBSDV, RBSDV, and RSV undergo LLPS to form dynamic membraneless droplets. In SRBSDV P6 droplets, a large number of host proteins, including many stress-related proteins, were identified. For example, the AGO18 protein, a core RNA silencing component involved in rice antiviral defense[21], was found in the droplets. Previous study reported that viral silencing suppressors can interfere with the assembly of the RNA-induced silencing complex (RISC) by hijacking key RISC assembly factors, thereby suppressing the antiviral defense[70]. SRBSDV P6 protein may sequester AGO18 within membraneless droplets, thereby impairing rice antiviral immunity of RNA silencing. Further studies are needed to explore the roles of AGO18 in P6-formed droplets. Furthermore, among these identified host proteins, OsTSN1 was highly enriched and drew our attention (Supplementary Data 1). OsTSN1 harbors three IDRs and forms droplets in vitro under PEG-8000 treatment (Fig. 2i). However, the assembly of OsTSN1 droplets in vivo is strictly dependent on specific stress conditions, including heat shock, salt stress or the presence of SRBSDV P6 (Figs. 2h, 3c and Supplementary Fig. 6b, c). Based on these findings, we speculate that TSN1 is not able to form droplets alone in plants, probably due to the presence of some plant-inhibiting factors. In general, the formation of RNA granules such as SGs and PBs is considered an antiviral stress response in host cells during virus infection[71]. Thus, redirecting RNA membraneless condensate components and disrupting these structures serve as strategies utilized by viruses to facilitate their replication and evade host defenses[72,73]. Here, we demonstrated that SRBSDV P6 protein interacts with OsTSN1 to form droplets primarily localized at SGs with a smaller fraction in PBs (Fig. 4). Although SGs and PBs are considered distinct organelles, a percentage of SGs and PBs are found "docked" against one another upon SG assembly[74]. The localization relationship between P6-OsTSN1 droplets and SGs/PBs suggests the potential existence of a dynamic material exchange between SGs and PBs. Notably, other viral proteins were also detected within P6 droplets (Supplementary Data 1). We speculate that P6 manipulates the composition of these biomolecular condensates by recruiting both host and viral proteins, thereby weakening plant defense response and establishing viral factories to support virus multiplication. Further investigation is required to elucidate the roles of viral and host proteins within these condensates. Additionally, future studies are needed to explore the differences in proteins and bound RNAs from virus-induced and abiotic stress-induced SGs and the distinct roles of these SGs in plant stress responses.

In this work, we confirmed that nuclease protein OsTSN1 can degrade ssRNAs, but not dsRNAs or SRBSDV genomic RNA (Supplementary Fig. 10c–e). Similar to *Arabidopsis* TSN protein[75], the nuclease activity of OsTSN1 depends on the SN domains in the N-terminus (Supplementary Fig. 10d, e). Moreover, nuclease activity of OsTSN1 is positively correlated with its multimerization degree (Supplementary Fig. 11). High concentration of glutaraldehyde or DTT can depolymerize the OsTSN1 multimer, thereby inactivating its nuclease activity (Supplementary Fig. 11), indicating that OsTSN1 requires a certain spatial conformation for its enzymatic activity. LLPS driven by SRBSDV P6 enhances the nuclease activity of OsTSN1 via promoting its multimerization within droplets (Fig. 5). This may explain why the droplets increase in size with the rising concentration of P6. In *Arabidopsis*, the nuclease activity of TSN, driven by the tandem repeat of four SN domains, is essential for its targeting to SG[48]. Whether the P6-OsTSN1 droplets rely on the nuclease activity of the SN domains in OsTSN1 to localize at SGs, and how SGs, in turn, influence the P6-OsTSN1 droplets, remains to be investigated.

In general, RBPs are known as the key regulatory proteins of RNA expression in plant cells[76,77]. Current knowledge indicates that the RNA-binding activity of certain unorthodox RBPs is critical for virus infection[78,79]. OsTSN1, as an RBP, is essential for storage protein expression, seed development, and protein body formation[80]. However, the role of OsTSN1 in regulating rice host RNAs during virus infection has not yet been explored. In this work, we demonstrated that OsTSN1 can bind preferentially to the coding regions of mRNAs with G-A-rich motifs; in P6-OsTSN1 droplets, the highly enriched mRNAs are mostly TFs, including NAC, MYB-related, and bZIP TF family members. These TFs are known to play roles in plant development and responses to biotic stresses, including virus infection[81]. As expected, the transcription levels of six targeted mRNAs by OsTSN1 are significantly down-regulated in SRBSDV-infected rice and P6-OE transgenic plants, but up-regulated in ostsn1 knockout mutant plants (Supplementary Fig. 17a–c), indicating that the TF mRNAs are targeted and degraded in P6-induced OsTSN1 droplets localized at SGs. On the contrary, viral transcripts of SRBSDV were not found in OsTSN1-targeting RNAs (Supplementary Data 3), indicating that there is selectivity in which transcripts are bound by OsTSN1 in P6-OsTSN1 droplets. How the P6-OsTSN1 droplets select target RNAs remains to be investigated.

Symptom observation and virus accumulation analyses indicated that osnac15 and oslhy mutant plants were more susceptible to SRBSDV (Fig. 6), suggesting that *OsNAC15* and *OsLHY* participate in host defense responses against SRBSDV infection. However, to date, the potential role of OsLHY and OsNAC15 in defending against virus infection has not been investigated. Here, we found that OsLHY is a transcriptional repressor and can bind to the promoters of genes involved in the JA signaling pathway, namely *JAZ6*, *JAZ12*, and *JAZ15*, to suppress their expression. On the other hand, the autophagy-related *OsATG8C* is positively regulated by the TF OsNAC15 (Fig. 7). Autophagy and jasmonate (JA)-associated hormone pathways are well-known important plant antiviral defense systems[20,82–84]. The degradation of *OsLHY* transcript in P6-OsTSN1 droplets contributes to the elevation of expression levels of *JAZ6* and *JAZ12*, presumably leading to the

https://doi.org/10.1038/s41467-025-62395-5

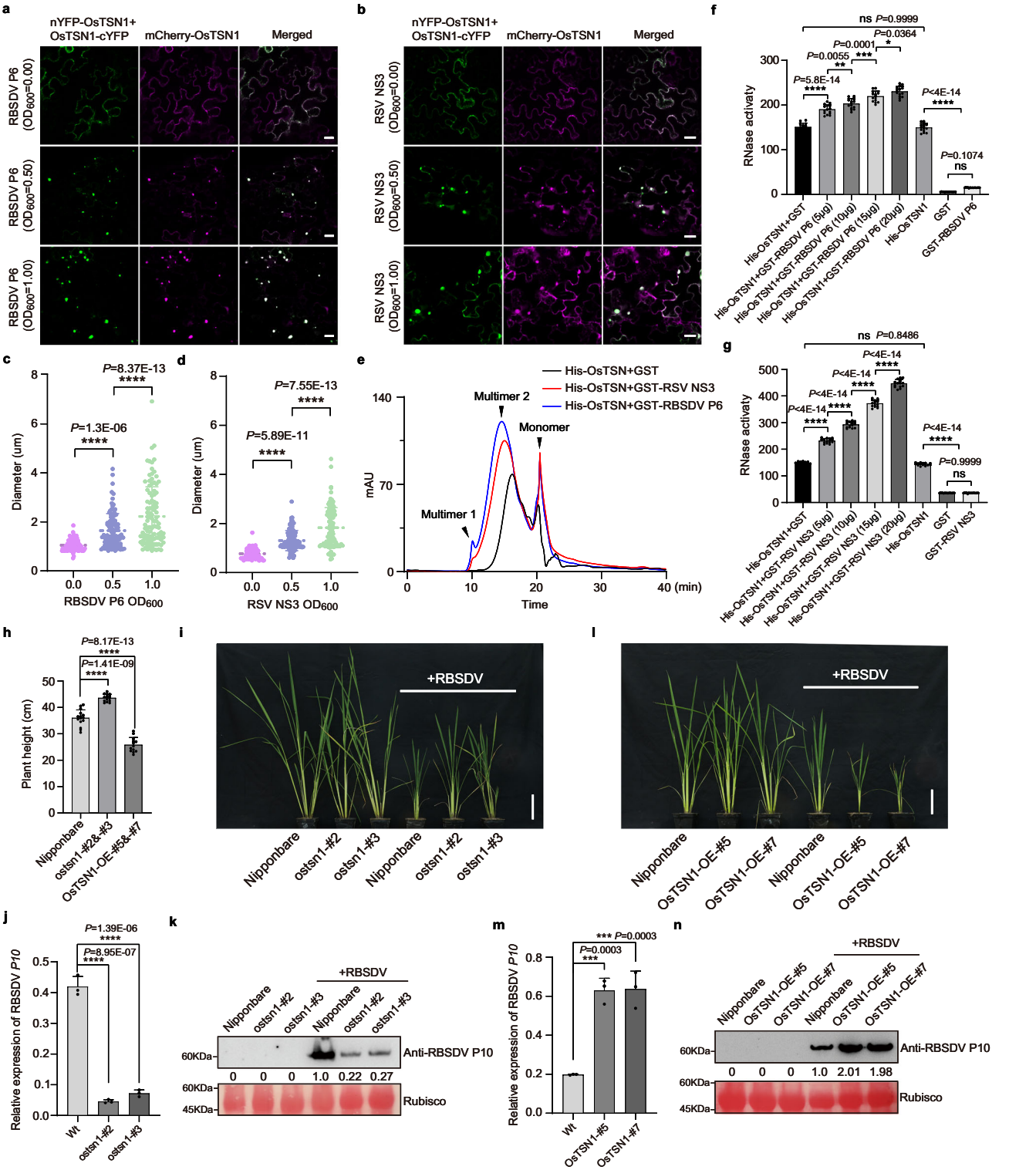

suppression of the MYC2-related JA signaling. Meanwhile, the transcriptional level of *OsATG8C* declines due to the cleavage of its TF gene, *OsNAC15*, which would impair the rice host's antiviral autophagy-associated response (Fig. 8). Nevertheless, the function of other downstream genes targeted by the other four TFs identified in the P6-OsTSN1 condensates is currently unclear.

Several previous reports have indicated that different plant RNA viruses and their viral proteins can convergently target host factors to enhance their infection in plants[85,86]. In this study, we discovered that, similar to SRBSDV P6, both RBSDV P6 and RSV NS3 contain IDRs and interact with OsTSN1 to form membraneless droplets localized in SGs. This interaction leads to enhanced nuclease activity of OsTSN1 (Fig. 9 and Supplementary Fig. 26). Furthermore, OsTSN1-OE transgenic rice plants are more susceptible to RBSDV and RSV infection than WT plants, whereas ostsn1 knockout mutant plants exhibit reduced susceptibility to these viruses (Fig. 9 and Supplementary Fig. 27). Thus, targeting TSN1 in rice breeding could offer a strategy for managing multiple virus infections in paddy fields.

Based on these findings, we propose a working model for the interplay between viral RNA silencing suppressors and OsTSN1 to

Fig. 9 | RBSDV P6 and RSV NS3 promote OsTSN1 multimerization and nuclease activity to facilitate virus infection. a, **b** Confocal microscope showing RBSDV P6 (**a**) and RSV NS3 (**b**) promote OsTSN1 multimerization and droplet formation in *N. benthamiana* leaf cells at 2 dpa. Scale bar, 20 μm. **c**, **d** Statistical analysis of the diameter size of RBSDV P6-OsTSN1 (**c**) and RSV NS3-OsTSN1 (**d**) droplets shown in **a** ($n = 103, 101, 103$ droplets, respectively) and **b** ($n = 100$ droplets), using the ImageJ software (1.53 v). The data are the means ± SD from three independent biological experiments, determined using the one-way ANOVA with Tukey's test. $^{****}P < 0.0001$. **e** SEC-HPLC profile of OsTSN1 multimers triggered by GST-RBSDV P6 or GST-RSV NS3 in vitro. The peaks of the monomer and multimers were indicated by black arrows. **f**, **g** Fluorometric assay results showing the nuclease activity of OsTSN1 regulated by RBSDV P6 (**f**) and RSV NS3 (**g**). Values are the mean ± SD ($n = 15$) from three independent experiments, determined using the one-way ANOVA with Tukey's test. ns, no significant statistical difference, $^{*}P < 0.05$, $^{****}P < 0.0001$. **h** Heights of RBSDV-infected WT, ostsn1 and OsTSN1-OE transgenic rice plants. The data are the means ± SD ($n = 15, 14, 13$, respectively) from three independent biological experiments, determined using the one-way ANOVA with Tukey's test. ns, no significant statistical difference, $^{****}P < 0.0001$. **i**–**n** Phenotypes of the uninfected or RBSDV-infected WT, ostsn1 knockout mutant plants (**i**) and OsTSN1-OE transgenic plants (**l**) at 30 dpi. Scale bar, 10 cm. RT-qPCR result showing the expression level of RBSDV *P10* in RBSDV-infected WT, ostsn1 knockout mutant plants (**j**) and OsTSN1-OE transgenic plants (**m**) at 30 dpi. The data are the means ± SD from three independent biological replicates, determined using a one-way ANOVA with Tukey's test. $^{***}P < 0.001$. $^{****}P < 0.0001$. Western blot result showing the accumulation level of RBSDV P10 in RBSDV-infected WT, ostsn1 knockout mutant plants (**k**) and OsTSN1-OE transgenic plants (**n**) at 30 dpi. The Rubisco bands are used to show equal loading. Experiments in (**a**, **b**, **k**, and **n**) were repeated three times with similar results.

benefit virus infection in rice plants (Fig. 10). In infected rice cells, viral RNA silencing suppressors, SRBSDV P6, RBSDV P6 and RSV NS3, undergo LLPS and interact with OsTSN1 to form P6-OsTSN1 and NS3-OsTSN1 droplets localized at SGs. In these droplets, all SRBSDV P6, RBSDV P6, and RSV NS3 promote multimerization and the nuclease activity of OsTSN1 to degrade transcripts of transcription factors OsLHY and OsNAC15, which are regulators of the JA- and autophagy-associated host immune pathways. This leads to suppressing the plant defense response against virus infection. In conclusion, we have shown evidence to support the notion that plant RNA viruses utilize their proteins to hijack host factors through LLPS and interfere with the host JA- and autophagy-associated immune pathways, which benefits their infection. These findings also allow us to better understand how plant viruses utilize LLPS to combat host immunity.

Methods

Plant growth and viral inoculation

OsTSN1 overexpression (OsTSN1-OE) and SRBSDV *P6* expression (P6-OE) transgenic Nipponbare (NPB) rice lines were generated as described previously[87]. The ostsn1 knockout mutant rice lines in NBP background and osnac90, osnac75, osnac15, ostga6, oslhy, osjaz6, osjaz12, osjaz15, and osatg8c knockout mutant rice lines in Zhong hua 11 (ZH11) background produced using the CRISPR/Cas9 method were purchased from the Biogle Genome Editing Center (Jiangsu, China). All assayed rice seedlings were grown inside a greenhouse maintained at 28–32 °C with natural sunlight. *N. benthamiana* plants were grown inside a growth room maintained at 23 °C and a 12 h light/12 h dark photoperiod. The virus inoculation assay was performed as previously described[88]. Briefly, nonviruliferous white-backed planthoppers (WBPHs) were allowed to feed on the SRBSDV-infected rice plants for 3 d and then transferred onto healthy rice seedlings. Twelve days later, WBPHs were tested for SRBSDV infection by dot-ELISA. The confirmed viruliferous WBPHs were then used to transmit SRBSDV on the three-leaf-stage rice seedlings for 2–3 d. In this experiment, each seedling was inoculated with two or three viruliferous WBPHs. Seedlings inoculated with SRBSDV-free WBPH were used as controls. After removing WBPHs, the inoculated rice plants were grown inside a greenhouse for disease symptom observations and virus accumulation assays. The incidence rates of inoculated rice plants were tested by dot-ELISA. The inoculation of RBSDV or RSV to rice seedlings was the same as described above, but SBPH was used as the transmission vector.

Plasmid constructions

For obtaining OsTSN1-OE and P6-OE transgenic rice lines, full-length coding sequences (CDSs) of *OsTSN1* and SRBSDV *P6* were cloned into the pCAMBIA1300 vector, driven by the CaMV 35S promoter with Flag-tag. To generate ostsn1, osnac90, osnac75, osnac15, ostga6, oslhy, osjaz6, osjaz12, osjaz15, and osatg8c knockout transgenic plants, the targeted sgRNA of these genes mentioned above were synthesized and were introduced into CRISPR plasmid BGK032 vectors (Biogle, Jiangsu, China). The rice transformation was carried by Biogle Genome Editing Center. For yeast-two-hybrid (Y2H) assays, full-length CDSs of *OsLHY*, *OsNAC15*, *OsTSN1* and its truncated mutants, *NbTSN1*, *NbTSN3*, *ZmTSN1* and SRBSDV *P6* and its site-directed mutagenized mutants or truncated mutants were RT-PCR-amplified from the SRBSDV-infected or non-infected rice or *N. benthamiana* plants using gene-specific primers (Supplementary Data 9). The amplified roducts were inserted individually into the yeast expression vector pGADT7 or pGBKT7 using an infusion cloning kit as instructed (Monad, Wuhan, China). For yeast-one-hybrid (Y1H) assays, a sense and a non-sense strand of a three-repeated AAGATATTT fragment or AGCAAGA fragment were synthesized and annealed together to form a double-stranded fragment, followed by insertion into the pHIS2 vector. Thirty bp sequence in promoters of *OsJAZ6*, *OsJAZ12*, *OsJAZ15* and *OsATG8C* containing the AAGATATTT or AGCAAGA motif was amplified and cloned into the pHIS2 vector. For pull-down and nuclease activity assays, the RT-PCR-amplified full-length SRBSDV *P6*, RBSDV *P6*, RSV *NS3* and *OsTSN1* CDSs were individually cloned into the prokaryotic expression vector pGEX4T-3, pET-32a or pMAL-c5E to produce vectors expressing GST-P6, GST-P6^{Q42A,Y57A}, GST-RSV NS3, His-P6, His-OsTSN1, and MBP-OsTSN1, respectively. For the droplet assembly assay, the CDSs of *RFP*, *GFP*, *RFP-P6*, *GFP-OsTSN1*, *RFP-IDR3*, and *RFP-P6*$^{\triangle IDR3}$ were separately cloned into the vector pET-32a to produce vectors expressing His-RFP, His-RFP-P6, His-GFP, His-GFP-OsTSN1, His-RFP-IDR3, and His-RFP-P6$^{\triangle IDR3}$, respectively. For the bimolecular fluorescence complementation (BiFC) assay, the CDSs of *OsTSN1* and its truncated mutants, the *P6* and its truncated mutants, RBSDV *P6*, RRSV *P6*, and RSV *NS3* were individually cloned into the n-YFP or c-YFP expression vector. For the subcellular localization assays, the CDSs of the *P6* and its truncated mutants, RBSDV *P6*, RSV *NS3*, *OsTSN1*, *NbG3BP*, *NbDCP1* and *NbTSN1* were separately cloned into the pGD or the pCambia vector with HA-, Flag-, GFP- or mCherry-tag, all behind the CaMV 35S promoter. For the luciferase reporter assays, the CDSs of *OsLHY* and *OsNAC15* were separately inserted into the pGreenII 62-SK vector to express the two effectors as reported[89]. A 2000 bp sequence representing the promoter of *OsJAZ6*, *OsJAZ12*, *OsJAZ15*, *OsATG8C* was inserted into the pGreenII 0800-LUC vector to generate reporter vectors. For the virus-induced gene silencing (VIGS) assays, we used a tobacco rattle virus (TRV)-based vector. A 300 bp fragment, representing a partial sequence of *NbTSN1&2* and *NbTSN3* was identified using the online VIGS tool (https://vigs.solgenomics.net), RT-PCR-amplified, and cloned into the pTRV2 vector via an infusion cloning method. Primers used in this study are listed in Supplementary Data 9.

Plant protein extraction and Western blot assays

Total protein was extracted from leaf tissues using a RIPA lysis buffer (Beyotime, Shanghai, China). Protein samples were pelleted through 3 min centrifugation at 12,000 × *g* and the supernatants were mixed with a 5× SDS loading buffer (Fdbio Science, Hangzhou, China)

https://doi.org/10.1038/s41467-025-62395-5

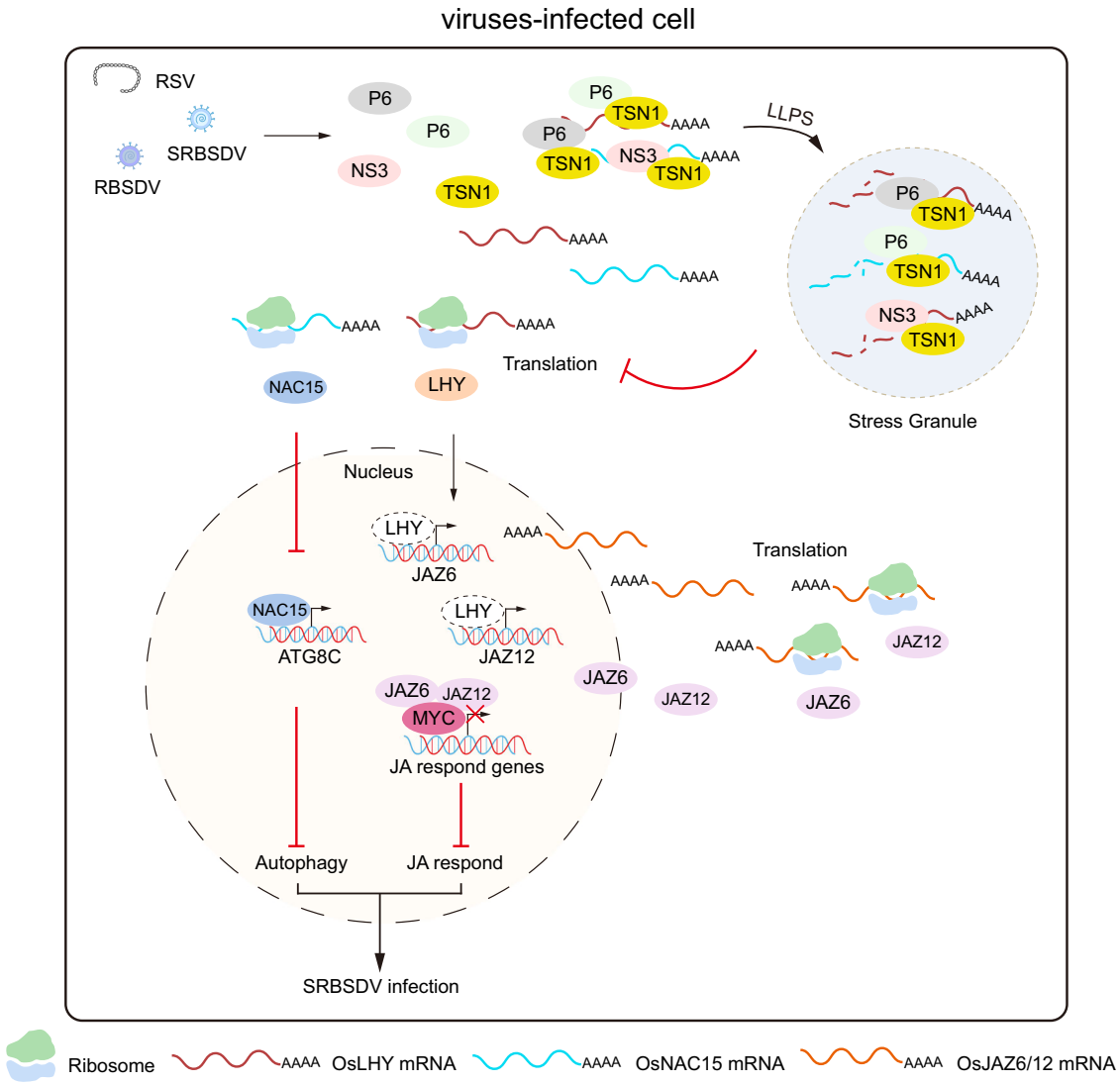

Fig. 10 | A working model showing how viral proteins encoded by rice-infecting viruses utilize OsTSN1 to disturb the JA- and autophagy-associated plant immunity via RNA decay. In infected rice cells, viral RNA silencing suppressors (SRBSDV P6, RBSDV P6 and RSV NS3) undergo LLPS and interact with OsTSN1 to form viral protein-OsTSN1 droplets localized in SGs, which promote multimerization and the nuclease activity of OsTSN1 to degrade transcripts encoding two transcription factors OsLHY and OsNAC15, thereby suppressing the downstream JA- and autophagy-associated rice immune pathway to facilitate virus infection. The schematic diagram was created in BioRender. Zeng, M. (2025) https://BioRender.com/i3oh1p0.

followed by 10 min boiling. The resulting protein samples were analyzed through SDS-PAGE. An anti-OsTSN1 rabbit polyclonal antibody, and anti-SRBSDV P10, anti-RBSDV P10, and anti-RSV CP monoclonal antibodies were produced in authors' laboratory[90]. The His-tag, GFP-tag, mCherry-tag, and Flag-tag antibodies were purchased from ABclonal (Wuhan, China), the GST-tag, MBP-tag, and HA-tag antibodies were purchased from Beyotime (Shanghai, China). All the above antibodies were diluted to 1:5000 (v/v) and used as the primary antibodies. Horse radish peroxidase (HRP)-conjugated secondary antibodies (Sigma-Aldrich, Taufkirchen, Germany) were diluted to 1:8000 (v/v) prior to nitrocellulose membrane probing. The resulting membranes were treated with an ECL substrate solution (Fdbio science), and imaged using the ImageQuant LAS 4000mini system (GE HealthCare, Illinois, USA). The expression levels of actin or rubisco were used to show sample loadings. The intensities of protein bands were quantified using the ImageJ software (NIH, Bethesda, Maryland, USA).

Y2H, Y1H, and transcription factor-centered Y1H assays

The Y2H assays were performed according to the protocol in the Matchmaker Gold Yeast-two-hybrid system (Clontech, SanJose, CA, USA). The different expression vector combinations were co-transformed into the yeast strain Gold cells. The transformed cells were screened on a selective SD double-dropout medium (SD-Leu-Trp) for 3 d at 30 °C, and the positive colonies were grown on the SD triple-dropout medium (SD-His-Leu-Trp) for 3 d at 30 °C and then on the SD quadruple-dropout medium (SD-Ade-His-Leu-Trp) for another 3 d at 30 °C. The Y1H assay was performed using the Matchmaker Gold Yeast-one-hybrid System as instructed (Clontech). Briefly, plasmids pGADT7-OsLHY and pGADT7-OsNAC15 were individually co-transformed with a recombinant or empty pHIS2 vector into the yeast strain Y187 cells. The transformed cells were grown on a medium lacking Leu and Trp (SD-Leu-Trp) for 3 d at 30 °C. The transformants were then grown on a medium lacking Leu, Trp, and His (SD-His-Leu-Trp) supplemented with 100 or 150 mM 3-Amino-1,2,4-triazole (3-AT, Sangon Bioech, Shanghai, China) for another 3 d at 30 °C. The transcription factor-centered Y1H assay was performed as previously described[91]. Briefly, the yeast strain Y187 motif library (Nanjing Ruiyuan Biotechnology Co. Ltd., Nanjing, China) was incubated overnight at 28 °C. The resulting yeast cells were collected and used to produce competent cells using the Lithium acetate. Plasmid pGADT7-OsNAC15 (20 μg) was transformed into the

competent library cells, and the re-transformed yeast cells were grown on the SD-Trp-Leu-His medium supplemented with 100 mM 3-AT for 5 d at 30 °C. After PCR verification, the positive colonies were selected, and the inserts in these positive colonies were sequenced and analyzed using the FIMO website (https://meme-suite.org/meme/).

Transactivation activity assay

The transactivation activity assay was performed as previously described with some modifications[92]. Briefly, pGBKT7-OsNAC15 and pGBKT7-OsLHY plasmids were individually co-transformed with pGADT7-Rec vector (Clontech) into yeast strain Y187 cells. The transformed cells were grown on the SD-Leu-Trp medium for 3 d at 30 °C. The transformants were then grown on the SD-Ade-His-Leu-Trp medium to determine the transactivation activity in yeast. The cells co-transformed with pGBKT7-NbARF17 and pGADT7-Rec vector were used as a positive control, and the cells co-transformed with pGBKT7 and pGADT7-Rec vector were used as a negative control.

Immunoprecipitation coupled with mass spectrometry

The immunoprecipitation assay was performed as previously described[93]. Briefly, leaf samples (10 g each) were collected from 30-day-old SRBSDV-infected or non-infected rice plants and frozen in liquid nitrogen. After grinding, each sample was homogenized in 30 mL of a lysis buffer [50 mM Tris-Cl (pH7.6), 200 mM NaCl, 5 mM $MgCl_2$, 10% glycerol, 0.5% Nonident P 40, 0.5 mM 1,4-Dithiothreitol (DTT, Sangon Biotech), 1 mM phenylmethyl sulfonyl fluoride (PMSF, Sangon Biotech), and one tablet of protease inhibitor cocktail (Sigma-Aldrich)]. The mixture was incubated for 30 min at 4 °C followed by 15 min centrifugation at 14,000 × *g* and 4 °C. The resulting supernatant was incubated with Protein G Magnetic Beads (Millipore, Billerica, USA) for 1 h to remove non-specifically adsorbed proteins, followed by removing the Protein G Magnetic Beads. Then, each treated supernatant was incubated with an anti-SRBSDV P6 monoclonal antibody previously developed in author's laboratory[53] at 4 °C for 4 h. Fresh Protein G Magnetic Beads were rinsed three times with the lysis buffer and then added to the above lysate followed by 2 h incubation at 4 °C. The bead-protein mixture was washed five times with the lysis buffer and then boiled in the 2× SDS-PAGE loading buffer. After SDS-PAGE and silver staining, the protein bands that were present in SRBSDV-infected rice but not in uninfected rice were collected as one sample and analyzed through mass spectrometry by the Analysis Center of Agrobiology and Environmental Sciences, Zhejiang University (Hangzhou, China). The extracted peptides were analyzed using Proteome Discoverer (version 3.1) with default parameters. Protein identification was performed using Blast searches against the SRBSDV protein databases (https://www.ncbi.nlm.nih.gov/) and the Rice Genome Annotation Project database (https://rice.uga.edu/). The raw MS data were deposited to the ProteomeXchange Consortium via the PRIDE partner repository with the dataset identifier PXD059146.

In vitro pull-down assay

For pull-down assay, pGEX4T-3-P6, pGEX4T-3-P6^{Q42A,Y57A}, pGEX4T-3-RSV NS3, pET-32a-RBSDV P6, pET-32a-OsTSN1, and pMAL-c5E-OsTSN1 vectors were separately transformed into *Escherichia coli* strain BL21 (DE3) cells. The cells transformed with the empty pGEX4T-3 or pMAL-c5E vector were used as the controls. The expressed proteins were purified from the cells using the Glutathione Resin (GenScript, Nanjing, China), High Affinity Ni-TED Resin (GenScript) or Dextrin Beads (Smart-Lifesciences, Changzhou, China). For each pull-down assay, 20 μg GST-P6, GST-RSV NS3 or His-RBSDV P6 was mixed with 20 μg MBP-OsTSN1 or His-OsTSN1. The protein samples mixed with 20 μg GST-tag or MBP-tag were used as the negative controls. The mixed protein samples were incubated with the Glutathione Resin or Dextrin Beads at 4 °C for 2 h and then pelleted through 5 min centrifugation at 1500 × *g* and 4 °C. The pelleted resin or beads were gently washed five times in the pull-down buffer [20 mM Tris-Cl (pH 8.0), 100 mM NaCl, 0.5 mM EDTA, and 0.5% (v/v) NP-40] and then boiled for 10 min in the 5× SDS-PAGE loading buffer. An anti-His (ABclonal), anti-GST (Beyotime) or anti-MBP (Beyotime) antibody was used to probe the Western blot membranes. For each competitive binding pull-down assay, 50 μg MBP-OsTSN1 was first mixed with 50 μg His-OsTSN1 and then with 50 μg GST or 50 μg GST-P6^{Q42A,Y57A} or GST-P6 (5, 10, 25 or 50 μg). The reaction containing GST or GST-P6^{Q42A,Y57A} was used as the negative control. Dextrin beads were added to each reaction and incubated overnight at 4 °C. After 5 min centrifugation at 1500 × *g* and 4 °C, the beads were washed five times in the pull-down buffer and boiled for 10 min in the 5× SDS-PAGE loading buffer. After electrophoresis, the nitrocellulose membranes were analyzed with an anti-His (ABclonal), anti-GST (Beyotime) or anti-MBP (Beyotime) antibody.

BiFC assay

Plasmids expressing nYFP-P6, nYFP-RBSDV P6, nYFP-RSV NS3, nYFP-OsTSN1, OsTSN1-cYFP, nYFP-Gus, Gus-cYFP, N-OsTSN1$^{\triangle SN1}$-cYFP, N-OsTSN1$^{\triangle SN2}$-cYFP, N-OsTSN1$^{\triangle SN3}$-cYFP and N-OsTSN1$^{\triangle SN4}$-cYFP, were transformed individually into *A. tumefaciens* strain EHA105 cells through electroporation. The *A. tumefaciens* cultures were mixed in specific combinations and co-infiltrated into *N. benthamiana* leaves. The infiltrated leaves were harvested at 48 h post infiltration (hpi) and examined under an FV3000 Olympus confocal microscope (Olympus, Tokyo, Japan).

In vitro droplet assembly assays and FRAP assays

Prokaryotically expressed His-RFP, His-RFP-P6, His-GFP, His-GFP-OsTSN1, His-RFP-IDR3, and His-RFP-P6$^{\triangle IDR3}$ were individually purified with the Ni-TED beads (GenScript) as instructed. Droplet assembly assays were performed using a droplet buffer [20 mM HEPES (pH 7.4), 50 mM KCl, and 8% (v/v) PEG-8000]. The resulting droplets were observed and imaged under a FV3000 Olympus confocal microscope. To investigate the recovery of the protein after photobleaching, protein droplets were photobleached with a full-strength laser with a 488/561-nm wavelength. The fluorescence signal was then recorded in a 2 s interval. For in vivo assays, over five droplets in different cells per treatment were examined, while for in vitro assays, over six droplets per treatment were examined. The resulting data curves were generated using the FV31S-SW software.

RNA extraction and RT-qPCR

Total RNA was extracted from leaf samples using TRIzol Reagent (Takara, Kyoto, Japan) and then treated with DNase I (Vazyme, Nanjing, China), followed by reverse transcription using the HiScript II Q Select RT SuperMix Kit (Vazyme). Quantitative PCR was performed using ChamQ SYBR Color qPCR Master Mix Kit (Vazyme) on a LightCycler 480 system (Roche, Basel, Switzerland). At least three independent biological replicates were used to represent one treatment, and three technical replicates were used for each biological sample. The expression levels of *OsUBQ5* and *NbActin* were used as the internal controls[86,94]. Primers used in this study are listed in Supplementary Data 9.

CLIP-seq and bioinformatic analysis

CLIP-seq was performed as previously described with minor modifications[93]. Briefly, tissues were collected from 30-day-old SRBSDV-infected or non-infected rice plants, immersed in ice-cold PBS buffer, and cross-linked with a 254 nm UV light for 30 min. The tissues were then ground in liquid nitrogen and extracted for total protein in the lysis buffer [20 mM Tris-HCl (pH 7.6), 300 mM KCl, 5 mM $MgCl_2$, 5 mM DTT, 0.5% (v/v) Triton X-100, 5% (v/v) glycerol, 1 mM PMSF) supplemented with 1 U/μL RNase inhibitor (Vazyme) and 1 tablet of cocktail protease inhibitor]. After clearing with Protein G Magnetic Beads, the supernatants were immunoprecipitated with an anti-OsTSN1 antibody and Protein G magnetic beads (Millipore).

Supernatant precipitated with the rabbit IgG (Vazyme) and Protein G magnetic beads (Millipore) were used as the negative control. After immunoprecipitation, the RNA-protein-bead complexes were rinsed five times in the lysis buffer and then eluted with an elution buffer [50 mM Tris (pH 6.8), 5% SDS] within a 20 min period at 55 °C. The resulting RNA-protein-bead complexes were treated with proteinase K (Beyotime) and DNase I at 50 °C for 15 min and then extracted using TRI-Reagent® (Invitrogen, Massachusetts, USA). RNA sequencing library was constructed using the KC-Digital Stranded mRNA Library Prep Kit for Illumina® (Wuhan Seqhealth Co., Ltd., China) following the manufacturer's instructions and sequenced on a Novaseq 6000 sequencer (Illumina) equipped with a PE150 model. The clean reads were mapped to the reference genome of *O. sativa* L. *japonica* at the NCBI using the STAR software (version 2.5.3a) with default parameters. The R package exomePeak software was then used to find peak callings, and the peaks were presented using the Integrative Genomics Viewer (IGV) software (https://www.igv.org/). Sequence motifs enriched in the peak regions were identified using the Homer known motif enrichment software (Homer, http://homer.salk.edu/homer/configureHomer.pl). GO and KEGG enrichment analysis were performed using the KOBAS software (http://bioinfo.org/kobas). For CLIP-RT-qPCR, the purified RNA from CLIP was used to perform the qPCR. Primers used for CLIP-qPCR are listed in Supplementary Data 9. The raw data of CLIP-seq were deposited in the NCBI database under the primary GEO accession number GSE283861.

RNA-seq and analysis

Total RNA samples were collected from WT, P6-OE, uninfected and SRBSDV-infected rice plants (three replicates per sample). Library constructions and 2 × 150 paired-end RNA sequencing in Illumina HiSeq 1000 were performed by Azenta Co., Ltd. (Beijing, China). After the quality assessment of raw reads by FastQC software (v0.12.0), the adaptor and low-quality reads were removed using Trimmomatic software (v0.38). The clean reads were mapped to the reference genome of *O. sativa* L. *japonica* (https://www.ncbi.nlm.nih.gov/) using Tophat (v1.4.6). Gene expression levels were calculated as fragments per kilobase per million reads (FPKM) by HTSeq (v0.6.1), and DEseq2 was used to analyze differentially expressed genes with the criteria of FC > 0.5 and adjusted $P < 0.05$. The raw data of RNA-seq were deposited in the NCBI database under the primary GEO accession number GSE283860.

Isolation of stress-induced SGs

Extraction of SGs from *N. benthamiana* leaf cells was performed as reported previously[95]. Briefly, 48 h post-agroinfiltration, the assayed *N. benthamiana* plants were heated at 42 °C for 30 min. Leaf tissues (6 g) were collected from the assayed plants and homogenized in 5 mL cold SG lysis buffer [50 mM Tris-HCl (pH7.4), 100 mM potassium acetate, 2 mM magnesium acetate, 0.5 mM DTT, 1 mM NaF, 1 mM Na_3VO_4, 0.5% (v/v) NP-40, one tablet of protease inhibitor cocktail, and 1 U/μL RNase Inhibitor] in precooled mortars. The slurry was centrifuged at 4000 × *g* for 10 min at 4 °C, and the pellet was resuspended in 4 ml lysis buffer. About 500 μL sample was saved as the input sample, and the remaining sample was centrifuged at 18,000 × *g* for 10 min at 4 °C. The resulting pellet was resuspended again in 500 μL lysis buffer and centrifuged at 18,000 × *g* for 10 min at 4 °C. The pellet was resuspended in 500 μL lysis buffer and centrifuged at 850 × *g* for 10 min at 4 °C. The supernatant, which contained isolated SGs was examined under a confocal microscope and then analyzed through western blot assays using an anti-GFP (ABclonal), anti-mCherry (ABclonal) or anti-Flag (ABclonal) antibody.

Electrophoretic mobility shift assay

For the DNA EMSA assays, biotin-labeled and unlabeled single-stranded oligonucleotide probes were synthesized by Tsingke Biotech Co., Ltd., (Beijing, China), and were subsequently converted into double-stranded nucleotide probes through an annealing process. The purified prokaryotically expressed His-OsNAC15 or His-OsLHY (4 μg) was incubated with a biotin-labeled (40 nM), unlabeled (0.2–10 μM) or a mutant probe (0.4–8 μM) in a 10 μL EMSA/Gel-Shift buffer (Beyotime) for 1 h at 25 °C. The mixtures were then analyzed in 4% polyacrylamide gels through electrophoresis in a 0.5× TBE buffer (44.6 mM Tris, 44.5 mM boric acid, and 1 mM EDTA). After transferring to Hybond $^{N+}$ nylon membranes (GE Healthcare) and UV cross-linking, the probes were detected using an HRP-conjugated streptavidin (Beyotime). For the RNA EMSA assay, biotin-labeled and unlabeled RNA probe (40 nM) was synthesized by Tsingke Biotech Co., Ltd. (Beijing, China) and incubated with the purified prokaryotically expressed His-tag or His-OsTSN1 (4 μg) in a 10 μL binding buffer [10 mM HEPES (pH 7.3), 1 mM $MgCl_2$, 20 mM KCl, and 1 mM DTT] for 2 h at 4 °C. For competition assays, the above mixtures were simultaneously and additionally incubated with different concentrations of the unlabeled RNA probe or mutant RNA probe, then separated in 4% polyacrylamide gels, and transferred onto Hybond $^{N+}$ nylon membranes. After UV cross-linking, the RNA probes were detected using an HRP-conjugated streptavidin (Beyotime).

In vitro RNA pull-down assay

The biotin-labeled RNA probe was synthesized in vitro using a T7 High Yield RNA Transcription Kit (Vazyme) and the Biotin RNA Labeling Mix (Roche). The synthesized RNA probe was dissolved in an RNA-binding buffer [10 mM Tris-Cl (pH7.0), 10 mM $MgCl_2$, and 100 mM KCl]. The purified recombinant His-OsTSN1 or His-tag (2 μg) was incubated with the probe for 2 h at 4 °C. Streptavidin magnetic beads (Beyotime) were added to the above mixtures, followed by overnight incubation at 4 °C. The beads were washed five times in a washing buffer [10 mM Tris-Cl (pH7.0), 10 mM $MgCl_2$ and 300 mM KCl], boiled for 10 min in the 5× SDS-PAGE loading buffer, and the resulting products were then analyzed through Western blot assays using an anti-His antibody.

Extraction of SRBSDV gRNA

Extraction of dsRNA from SRBSDV-infected rice was performed using our established cellulose powder method. Firstly, after two Miracloth membranes and a filter disc were placed at the bottom of the central filter column, 250 mg of cellulose powder C6288 (Sigma-Aldrich) was added, and then the central filter column containing cellulose powder was placed in a 2 mL centrifuge tube to prepare the micro-spin column device. SRBSDV-infected plant tissue (80 mg) was ground in liquid nitrogen, then suspended in 500 μL of the nucleic acid extraction buffer [1% SDS, 0.1% β-mercaptoethanol, 2 mmol/L EDTA (pH8.0), 200 mmol/L NaCl, 20 mmol/L Tris-HCl (pH8.0)] and 10 mg of polyvinylpolypyrrolidone (PVPP, Sangon Biotech) in 2 mL centrifuge tube. Then phenol–chloroform–isoamyl alcohol (the volume ratio of 25:24:1, 500 μL) was added to the above crude extract and vortexed for 1 min followed by centrifuging at 20,000 × *g* for 5 min. About 400 μL supernatant was collected, and 80 μL of ethanol was added (the final concentration of 16.6%) and mixed well. The mixture was centrifuged at 20,000 × *g* for 3 min, and the resulting supernatant was transferred to the pre-prepared micro-spin column device. The column was centrifuged at 10,000 × *g* for 5 s and washed three times with wash buffer [16% ethanol, 1 mmol/L EDTA (pH8.0), 100 mmol/L NaCl, 10 mmol/L Tris-HCl (pH8.0)]. Then 400 μL of the elution buffer [1 mmol/L EDTA (pH8.0), 100 mmol/L NaCl, 10 mmol/L Tris-HCl (pH8.0)] was added to the column, followed by centrifuging at 10,000 × *g* for 5 s. The eluted fraction containing dsRNA was mixed with 40 μL of 3 M aqueous sodium acetate (pH 5.2) and 1 mL of ethanol to purify dsRNA, and placed at −20 °C for 10 min. After centrifuging at 20,000 × *g* for 5 min, the precipitated dsRNA sample was then dissolved in 20 μL of the elution buffer.

Nuclease activity assay

This assay was performed as previously described with minor modifications[53]. Briefly, single-stranded *eGFP*, *OsNAC15*, and *OsLHY* RNAs and double-stranded *eGFP* were separately transcribed in vitro using the T7 High Yield RNA Transcription Kit (Vazyme) and the T7 RNAi Transcription Kit (Vazyme). SRBSDV gRNA was extracted from SRBSDV-infected rice. Then the RNAs, served as substrates, were co-incubated individually with the purified recombinant His-OsTSN1 or its truncated mutants, different combinations of GST-SRBSDV P6, GST-RBSDV P6, GST-RSV NS3 or GST-tag in a reaction buffer [50 mM HEPES (pH7.0), 100 mM NaCl, 5 mM DTT, 5 mM $CaCl_2$, and 10% (v/v) glycerol] for 1 h at 28 °C. Following incubations, the integrity of ssRNA and dsRNA was assessed through electrophoresis in denatured agarose gels. For the quantitative assay, different amounts of purified recombinant GST-tag, GST-SRBSDV P6, GST-RBSDV P6 or GST-RSV NS3 were incubated with His-OsTSN1, and the detection of nuclease activity was carried out using Ambion™ RNaseAlert™ QC Kit (Thermo Fisher, Massachusetts, USA) according to manufacturer's instructions. Fluorescence signal intensity from each sample was measured using the FlexStation 3 microplate reader (Molecular Devices, California, USA) set at the 490 (excitation)/520 nm (emission) wavelength, and was used to represent the nuclease activity.

Dual-luciferase (Dual-Luc) transient transcriptional activity assays

Dual-Luc assay was conducted as described previously[96]. The OsNAC15 and OsLHY were used, respectively, as the effectors; the pGreenII 0800-LUC vector harboring the promoter sequence (2000 bp) of *OsJAZ6*, *OsJAZ12*, *OsJAZ15*, or *OsATG8C* was used as the reporter. The effector and reporter vectors were individually transformed into *A. tumefaciens* strain GV3101 cells, and the resulting cultures were co-infiltrated, in different combinations, into the leaves of 4-week-old *N. benthamiana* plants. Two days later, a luciferin substrate (Promega, Madison, USA) solution was sprayed onto the infiltrated leaves. After 5 min incubation in the dark, the images of Luc signals were captured using Photek's HRPCS5 photon-counting camera system (East Sussex, United Kingdom). Then the LUC/REN ratio was measured using the dual-luciferase assay reagents (Promega) following the manufacturer's instructions.

Protoplast preparation and transfection

Protoplasts were isolated from rice seedlings as described previously[97]. Briefly, rice seedlings were first grown in the 1/2 MS medium and then cut into 0.5 mm wide strips. The strips were placed in a 0.6 M mannitol solution for 10 min, digested for 4 h in the dark using 1.5% Cellulase R-10 (Yakult, Tokyo Metropolis, Japan) and 0.75% Macerozyme R-10 (Yakult) in a solution containing 0.6 M mannitol,10 mM MES (pH 5.7), 10 mM $CaCl_2$, and 0.1% BSA. After removing the enzyme solution, a W5 solution [154 mM NaCl, 125 mM $CaCl_2$, 5 mM KCl, and 2 mM MES (pH 5.7)] was added to the samples. After passing through a 40 μm nylon mesh, protoplasts were collected through 3 min centrifugation at 211 × *g*. A W5 solution was used to wash protoplasts four times, and the protoplasts were collected by centrifugation at 211 × *g* for 3 min. The pellets were resuspended in MMG solution [0.4 M mannitol, 15 mM $MgCl_2$ and 4 mM MES (pH 5.7)]. For protoplast transfection, 100 μL protoplasts were mixed with 10 μg plasmid DNA, followed by the addition of 110 μL solution containing 40% (w/v) PEG-4000, 0.2 M mannitol, and 0.1 M $CaCl_2$. The mixture was incubated for 15 min in the dark. An equal volume of W5 solution was added slowly into the protoplast mixture and centrifuged at 211 × *g* for 3 min. The resulting protoplasts were resuspended in a WI solution [0.5 M mannitol, 20 mM KCl, and 4 mM MES (pH 5.7)] and cultured for 12 h at 28 °C in the dark.

SRBSDV inoculation of rice protoplast

Rice protoplasts were inoculated with virus crude extract of SRBSDV-infected rice tissues as described previously with minor modifications[98]. Briefly, 1 g of SRBSDV-infected plant tissue was collected and disinfected with 70% ethanol. After being mixed with the quartz sands and the extraction buffer (0.1 mol/L-Histidine, 0.01 mol/L MgCl2, pH 6.2), the plant tissue was ground into a homogenate. The homogenate was centrifuged at 2000 × *g* for 5 min at 4 °C, and the supernatant was transferred to a new centrifuge tube and then centrifuged at 5000 × *g* for 20 min at 4 °C. The resulting supernatant was the virus crude extract. About 500 μL of virus crude extract was added to 100 μL protoplasts, followed by mixing with 500 μL of PEG solution [40% (w/v) PEG-4000 and 0.01 M $CaCl_2$]. After adding 4.5 mL of solution [0.6 M mannitol and 0.01 M $CaCl_2$ (pH 5.6)], the mixture was incubated for 10 min at room temperature in the dark. Then an equal volume of W5 solution was added slowly into the mixture and centrifuged at 211 × *g* for 3 min. The resulting protoplasts were resuspended in a WI solution and cultured at 28 °C in the dark.

1,6-HD treatment

For rice seedings, 2-week-old uninoculated rice seedlings or inoculated rice seedlings were planted on the liquid 1/2 MS medium supplemented with 1% (w/v) 1,6-HD (Sigma-Aldrich) for 12 h. For rice protoplasts used in confocal observation, protoplasts were incubated in WI solution containing 1.0% 1,6-HD for 1 h, followed by rinsing with fresh WI solution prior to confocal microscopy observation. To assess the viability of 1,6-HD-treated rice protoplasts, we stained living protoplasts with 0.01% fluorescein diacetate (Sigma-Aldrich). Cell viability was expressed as the percentage of living protoplasts among total protoplasts. For SRBSDV-infected rice protoplasts used to analyze transcript levels of SRBSDV *P6* and *P10*, the protoplasts were incubated in WI solution supplemented with 0.5% or 1.0% 1,6-HD for 12 h, followed by RNA extraction and RT-qPCR analysis.

SEC-HPLC analysis

The purified recombinant His-OsTSN1 was treated with glutaraldehyde and DTT at varying concentrations, or incubated with purified recombinant GST-SRBSDV P6, GST-RBSDV P6, GST-RSV NS3 or GST for 4 h before SEC-HPLC analysis. The SEC-HPLC analysis was performed on an Agilent 1100 liquid chromatography instrument using a Waters Ultrahydrogel 500 chromatography column (7.8 × 300 mm, 10 μm). Eighty μL of each sample was injected per run. The mobile phase (pH 6.8) consisted of 0.05 M sodium phosphate and 0.2 M arginine hydrochloride. Each sample was eluted for 40 min at a flow rate of 0.5 mL/min. Protein elution was monitored by UV absorbance at 280 nm.

TRV-based VIGS assay

A. tumefaciens cultures harboring the pTRV1, pTRV2 or its derivatives were resuspended individually in the infiltration buffer till OD_{600} = 0.1. The cultures were mixed, in different combinations, at a 1:1 ratio (v/v), and co-infiltrated into *N. benthamiana* leaves. The gene silencing efficiency was determined through RT-qPCR at 8 days post-agroinfiltration.

Phylogenetic and statistical analyses

The phylogenetic tree was constructed using the MEGA 11 software with the maximum likelihood method with 1000 bootstrap replicates. The tree was presented using the iTOL tool (https://itol.embl.de/). Statistical analysis was performed using the two-tailed Student's *t* test or the one-way ANOVA with the Dunnett's multiple comparison test in the GraphPad Prism 8 package (GraphPad Software, California, USA).

Reporting summary

Further information on research design is available in the Nature Portfolio Reporting Summary linked to this article.

Data availability

The rice gene sequence data from the article can be found in the Rice Genome Annotation Project under the following accession numbers:

OsTSN1 (LOC_Os02g32350), OsTSN2 (LOC_Os04g32960), OsNAC15 (LOC_Os07g48550), OsLHY (LOC_Os08g06110), OsJAZ6 (LOC_Os03g28940), OsJAZ12 (LOC_Os10g25290), OsJAZ15 (LOC_Os03g27900), OsATG8C (LOC_Os08g09240), OsUBQ5 (LOC_Os10g39620); the *N. benthamiana* gene sequence data can be found in the SOL Genomics Network under the following accession numbers: NbG3BP (Niben101Scf03456g00002.1), NbDCP1 (Niben101Scf08515g00023.1), NbTSN1 (Niben101Scf02027g01022.1), NbTSN2 (Niben101Scf02581g03002.1), NbTSN3 (Niben101Scf07579g04003.1), and *Z. mays* gene sequence data can be found in the NCBI database under the following accession numbers: ZmTSN1 (NP_001313298). The authors declare that the data supporting the findings of this study are available within the paper and its supplementary files. A reporting summary for this paper is available as a supplementary file. The raw RNA-seq data and CLIP-seq data have been deposited in the NCBI database under primary GEO accession numbers GSE283860 and GSE283861. The mass spectrometry data of co-immunoprecipitation proteins were deposited to the ProteomeXchange Consortium via the PRIDE partner repository with the dataset identifier PXD059146. Source data are provided with this paper.

References

1. Majumdar, A., Sharma, A. & Belludi, R. Natural and engineered resistance mechanisms in plants against phytoviruses. *Pathogens* **12**, 619 (2023).
2. Bragard, C. et al. Status and prospects of plant virus control through interference with vector transmission. *Annu. Rev. Phytopathol.* **51**, 177–201 (2013).
3. Dietzgen, R. G., Mann, K. S. & Johnson, K. N. Plant virus-insect vector interactions: current and potential future research directions. *Viruses* **8**, 303 (2016).
4. Zhou, G., Xu, D., Xu, D. & Zhang, M. Southern rice black-streaked dwarf virus: a white-backed planthopper-transmitted fijivirus threatening rice production in Asia. *Front. Microbiol.* **4**, 270 (2013).
5. Wu, Z. et al. A systematic review of southern rice black-streaked dwarf virus in the age of omics. *Pest Manag. Sci.* **79**, 3397–3407 (2023).
6. Mao, Q. et al. New model for the genesis and maturation of viroplasms induced by fijiviruses in insect vector cells. *J. Virol.* **87**, 6819–6828 (2013).
7. Zhang, H. M., Chen, J. P. & Adams, M. J. Molecular characterisation of segments 1 to 6 of Rice black-streaked dwarf virus from China provides the complete genome. *Arch. Virol.* **146**, 2331–2339 (2001).
8. Li, J. et al. Interactions between the P6 and P5-1 proteins of southern rice black-streaked dwarf fijivirus in yeast and plant cells. *Arch. Virol.* **158**, 1649–1659 (2013).
9. Li, J. et al. Characterization of homologous and heterologous interactions between viroplasm proteins P6 and P9-1 of the fijivirus southern rice black-streaked dwarf virus. *Arch. Virol.* **160**, 453–457 (2015).
10. Jia, D. et al. Virus-induced tubule: a vehicle for rapid spread of virions through basal lamina from midgut epithelium in the insect vector. *J. Virol.* **88**, 10488–10500 (2014).
11. Liu, Y. et al. The P7-1 protein of southern rice black-streaked dwarf virus, a fijivirus, induces the formation of tubular structures in insect cells. *Arch. Virol.* **156**, 1729–1736 (2011).
12. Bai, F.-w et al. Phylogenetic analysis reveals that a dwarfing disease on different cereal crops in China is due to rice black streaked dwarf virus (RBSDV). *Virus Genes* **25**, 201–206 (2002).
13. Xu, Y., Fu, S., Tao, X. & Zhou, X. Rice stripe virus: exploring molecular weapons in the arsenal of a negative-sense RNA virus. *Annu. Rev. Phytopathol.* **59**, 351–371 (2021).
14. Collum, T. D. & Culver, J. N. The impact of phytohormones on virus infection and disease. *Curr. Opin. Virol.* **17**, 25–31 (2016).
15. Baulcombe, D. RNA silencing in plants. *Nature* **431**, 356–363 (2004).
16. Chen, X. & Rechavi, O. Plant and animal small RNA communications between cells and organisms. *Nat. Rev. Mol. Cell Biol.* **23**, 185–203 (2022).
17. Ding, P. & Ding, Y. Stories of salicylic acid: a plant defense hormone. *Trends Plant Sci.* **25**, 549–565 (2020).
18. Ge, L., Zhou, X. & Li, F. Plant-virus arms race beyond RNA interference. *Trends Plant Sci.* **29**, 16–19 (2024).
19. Verma, V., Ravindran, P. & Kumar, P. P. Plant hormone-mediated regulation of stress responses. *BMC Plant Biol.* **16**, 86 (2016).
20. Yang, M., Ismayil, A. & Liu, Y. Autophagy in plant-virus interactions. *Annu. Rev. Virol.* **7**, 403–419 (2020).
21. Yang, Z. et al. Jasmonate signaling enhances RNA silencing and antiviral defense in rice. *Cell Host Microbe* **28**, 89–103 (2020).
22. Huang, S., Zhu, S., Kumar, P. & MacMicking, J. D. A phase-separated nuclear GBPL circuit controls immunity in plants. *Nature* **594**, 424–429 (2021).
23. Jia, M., Chen, X., Shi, X., Fang, Y. & Gu, Y. Nuclear transport receptor KA120 regulates molecular condensation of MAC3 to coordinate plant immune activation. *Cell Host Microbe* **31**, 1685–1699.e1687 (2023).
24. Zavaliev, R., Mohan, R., Chen, T. & Dong, X. Formation of NPR1 condensates promotes cell survival during the plant immune response. *Cell* **182**, 1093–1108.e1018 (2020).
25. Yang, P. et al. G3BP1 is a tunable switch that triggers phase separation to assemble stress granules. *Cell* **181**, 325–345.e328 (2020).
26. Xu, M., Mazur, M. J., Tao, X. & Kormelink, R. Cellular RNA hubs: friends and foes of plant viruses. *Mol. Plant Microbe Interact.* **33**, 40–54 (2020).
27. Liu, Q., Liu, W., Niu, Y., Wang, T. & Dong, J. Liquid–liquid phase separation in plants: advances and perspectives from model species to crops. *Plant Commun.* **5**, 100663 (2023).
28. Solis-Miranda, J. et al. Stress-related biomolecular condensates in plants. *Plant Cell* **35**, 3187–3204 (2023).
29. Liu, C. et al. A proxitome-RNA-capture approach reveals that processing bodies repress coregulated hub genes. *Plant Cell* **36**, 559–584 (2024).
30. Mäkinen, K., Lõhmus, A. & Pollari, M. Plant RNA regulatory network and RNA granules in virus infection. *Front. Plant Sci.* **8**, 2093 (2017).
31. Zhang, Z. J. et al. CCR4, a RNA decay factor, is hijacked by a plant cytorhabdovirus phosphoprotein to facilitate virus replication. *eLife* **9**, e53753 (2020).
32. Hoffmann, G., López-González, S., Mahboubi, A., Hanson, J. & Hafrén, A. Cauliflower mosaic virus protein P6 is a multivalent node for RNA granule proteins and interferes with stress granule responses during plant infection. *Plant Cell* **35**, 3363–3382 (2023).
33. Hafrén, A., Lõhmus, A. & Mäkinen, K. Formation of potato virus A-induced RNA granules and viral translation are interrelated processes required for optimal virus accumulation. *PLoS Pathog.* **11**, e1005314 (2015).
34. Krapp, S., Greiner, E., Amin, B., Sonnewald, U. & Krenz, B. The stress granule component G3BP is a novel interaction partner for the nuclear shuttle proteins of the nanovirus pea necrotic yellow dwarf virus and geminivirus abutilon mosaic virus. *Virus Res.* **227**, 6–14 (2017).
35. Gutierrez-Beltran, E., Denisenko, T. V., Zhivotovsky, B. & Bozhkov, P. V. Tudor staphylococcal nuclease: biochemistry and functions. *Cell Death Differ.* **23**, 1739–1748 (2016).
36. Cázares-Apátiga, J. et al. The Tudor Staphylococcal nuclease protein of entamoeba histolytica participates in transcription regulation and stress response. *Front. Cell. Infect. Microbiol.* **7**, 52 (2017).
37. Gao, X. et al. Poly(A)(+) mRNA-binding protein Tudor-SN regulates stress granules aggregation dynamics. *FEBS J.* **282**, 874–890 (2015).

38. Zhu, L. et al. Characterization of Tudor-sn-containing granules in the silkworm, Bombyx mori. *Insect Biochem. Mol. Biol.* **43**, 664–674 (2013).
39. Callebaut, I. & Mornon, J. P. The human EBNA-2 coactivator p100: multidomain organization and relationship to the staphylococcal nuclease fold and to the tudor protein involved in Drosophila melanogaster development. *Biochem. J.* **321**, 125–132 (1997).
40. Tong, X., Drapkin, R., Yalamanchili, R., Mosialos, G. & Kieff, E. The Epstein-Barr virus nuclear protein 2 acidic domain forms a complex with a novel cellular coactivator that can interact with TFIIE. *Mol. Cell. Biol.* **15**, 4735–4744 (1995).
41. Elbarbary, R. A. et al. Tudor-SN-mediated endonucleolytic decay of human cell microRNAs promotes G(1)/S phase transition. *Science* **356**, 859–862 (2017).
42. Scadden, A. D. The RISC subunit Tudor-SN binds to hyper-edited double-stranded RNA and promotes its cleavage. *Nat. Struct. Mol. Biol.* **12**, 489–496 (2005).
43. Caudy, A. A. et al. A micrococcal nuclease homologue in RNAi effector complexes. *Nature* **425**, 411–414 (2003).
44. Yang, J. et al. Transcriptional co-activator protein p100 interacts with snRNP proteins and facilitates the assembly of the spliceosome. *Nucleic acids Res.* **35**, 4485–4494 (2007).
45. Sami-Subbu, R., Choi, S. B., Wu, Y., Wang, C. & Okita, T. W. Identification of a cytoskeleton-associated 120 kDa RNA-binding protein in developing rice seeds. *Plant Mol. Biol.* **46**, 79–88 (2001).
46. Chou, H. L., Tian, L., Kumamaru, T., Hamada, S. & Okita, T. W. Multifunctional RNA binding protein OsTudor-SN in storage protein mRNA transport and localization. *Plant Physiol.* **175**, 1608–1623 (2017).
47. Wang, C. et al. The cytoplasmic-localized, cytoskeletal-associated RNA binding protein OsTudor-SN: evidence for an essential role in storage protein RNA transport and localization. *Plant J.* **55**, 443–454 (2008).
48. Gutierrez-Beltran, E., Moschou, P. N., Smertenko, A. P. & Bozhkov, P. V. Tudor staphylococcal nuclease links formation of stress granules and processing bodies with mRNA catabolism in Arabidopsis. *Plant Cell* **27**, 926–943 (2015).
49. Gutierrez-Beltran, E. et al. Tudor staphylococcal nuclease is a docking platform for stress granule components and is essential for SnRK1 activation in Arabidopsis. *EMBO J.* **40**, e105043 (2021).
50. Frei dit Frey, N. et al. The RNA binding protein Tudor-SN is essential for stress tolerance and stabilizes levels of stress-responsive mRNAs encoding secreted proteins in Arabidopsis. *Plant Cell* **22**, 1575–1591 (2010).
51. Yan, C., Yan, Z., Wang, Y., Yan, X. & Han, Y. Tudor-SN, a component of stress granules, regulates growth under salt stress by modulating GA20ox3 mRNA levels in Arabidopsis. *J. Exp. Bot.* **65**, 5933–5944 (2014).
52. Liu, C. et al. An actin remodeling role for Arabidopsis processing bodies revealed by their proximity interactome. *EMBO J.* **42**, e111885 (2023).
53. Sundström, J. F. et al. Tudor staphylococcal nuclease is an evolutionarily conserved component of the programmed cell death degradome. *Nat. Cell Biol.* **11**, 1347–1354 (2009).
54. Zhao, Y. et al. A viral protein orchestrates rice ethylene signaling to coordinate viral infection and insect vector-mediated transmission. *Mol. Plant* **15**, 689–705 (2022).
55. Fang, X. D. et al. Host casein kinase 1-mediated phosphorylation modulates phase separation of a rhabdovirus phosphoprotein and virus infection. *eLife* **11**, e74884 (2022).
56. Fu, S. et al. An evolutionarily conserved C4HC3-type E3 ligase regulates plant broad-spectrum resistance against pathogens. *Plant Cell* **34**, 1822–1843 (2022).
57. Tian, F., Yang, D. C., Meng, Y. Q., Jin, J. & Gao, G. PlantRegMap: charting functional regulatory maps in plants. *Nucleic Acids Res.* **48**, D1104–d1113 (2020).
58. Zhang, B. et al. RiceTFtarget: a rice transcription factor-target prediction server based on coexpression and machine learning. *Plant Physiol.* **193**, 190–194 (2023).
59. Weirauch, M. T. et al. Determination and inference of eukaryotic transcription factor sequence specificity. *Cell* **158**, 1431–1443 (2014).
60. Ji, X. et al. A novel method to identify the DNA motifs recognized by a defined transcription factor. *Plant Mol. Biol.* **86**, 367–380 (2014).
61. Xiong, R., Wu, J., Zhou, Y. & Zhou, X. Characterization and subcellular localization of an RNA silencing suppressor encoded by Rice stripe tenuivirus. *Virology* **387**, 29–40 (2009).
62. Shin, Y. & Brangwynne, C. P. Liquid phase condensation in cell physiology and disease. *Science* **357**, eaaf4382 (2017).
63. Emenecker, R. J., Holehouse, A. S. & Strader, L. C. Emerging roles for phase separation in plants. *Dev. Cell* **55**, 69–83 (2020).
64. Mitrea, D. M. et al. Methods for physical characterization of phase-separated bodies and membrane-less organelles. *J. Mol. Biol.* **430**, 4773–4805 (2018).
65. Boccaccio, G. L., Thomas, M. G. & García, C. C. Membraneless organelles and condensates orchestrate innate immunity against viruses. *J. Mol. Biol.* **435**, 167976 (2023).
66. Li, H. et al. Phase separation in viral infections. *Trends Microbiol.* **30**, 1217–1231 (2022).
67. Lopez, N. et al. Deconstructing virus condensation. *PLoS Pathog.* **17**, e1009926 (2021).
68. Malinowska, M., Niedźwiedzka-Rystwej, P., Tokarz-Deptuła, B. & Deptuła, W. Stress granules (SG) and processing bodies (PB) in viral infections. *Acta Biochim. Pol.* **63**, 183–188 (2016).
69. Hoffmann, G. et al. Arabidopsis RNA processing body components LSM1 and DCP5 aid in the evasion of translational repression during Cauliflower mosaic virus infection. *Plant Cell* **34**, 3128–3147 (2022).
70. Csorba, T., Kontra, L. & Burgyán, J. Viral silencing suppressors: tools forged to fine-tune host-pathogen coexistence. *Virology* **479-480**, 85–103 (2015).
71. Poblete-Durán, N., Prades-Pérez, Y., Vera-Otarola, J., Soto-Rifo, R. & Valiente-Echeverría, F. Who regulates whom? An overview of RNA granules and viral infections. *Viruses* **8**, 180 (2016).
72. Lloyd, R. E. Regulation of stress granules and P-bodies during RNA virus infection. *Wiley Interdiscip. Rev. RNA* **4**, 317–331 (2013).
73. Dhillon, P. & Rao, C. D. Rotavirus induces formation of remodeled stress granules and P bodies and their sequestration in viroplasms to promote progeny virus production. *J. Virol.* **92**, e01363-18 (2018).
74. Youn, J. Y. et al. Properties of stress granule and P-body proteomes. *Mol. Cell* **76**, 286–294 (2019).
75. Li, C. L., Yang, W. Z., Shi, Z. & Yuan, H. S. Tudor staphylococcal nuclease is a structure-specific ribonuclease that degrades RNA at unstructured regions during microRNA decay. *RNA* **24**, 739–748 (2018).
76. Köster, T. & Meyer, K. Plant ribonomics: proteins in search of RNA partners. *Trends Plant Sci.* **23**, 352–365 (2018).
77. Lorković, Z. J. Role of plant RNA-binding proteins in development, stress response and genome organization. *Trends Plant Sci.* **14**, 229–236 (2009).
78. Garcia-Moreno, M., Järvelin, A. I. & Castello, A. Unconventional RNA-binding proteins step into the virus-host battlefront. *Wiley Interdiscip. Rev. RNA* **9**, e1498 (2018).
79. Kenesi, E., Carbonell, A., Lózsa, R., Vértessy, B. & Lakatos, L. A viral suppressor of RNA silencing inhibits ARGONAUTE 1 function by precluding target RNA binding to pre-assembled RISC. *Nucleic Acids Res.* **45**, 7736–7750 (2017).
80. Chou, H. L., Tian, L., Fukuda, M., Kumamaru, T. & Okita, T. W. The role of RNA-binding protein OsTudor-SN in post-transcriptional regulation of seed storage proteins and endosperm development. *Plant Cell Physiol.* **60**, 2193–2205 (2019).
81. Viswanath, K. K. et al. The role of plant transcription factors in the fight against plant viruses. *Int. J. Mol. Sci.* **24**, 8433 (2023).

82. He, Y. et al. Jasmonic acid-mediated defense suppresses brassinosteroid-mediated susceptibility to Rice black streaked dwarf virus infection in rice. *N. phytol.* **214**, 388–399 (2017).
83. Zhang, C. et al. Suppression of jasmonic acid-mediated defense by viral-inducible MicroRNA319 facilitates virus infection in rice. *Mol. Plant* **9**, 1302–1314 (2016).
84. Huang, X. et al. Rhabdovirus encoded glycoprotein induces and harnesses host antiviral autophagy for maintaining its compatible infection. *Autophagy* **20**, 275–294 (2024).
85. Zhang, H. et al. Distinct modes of manipulation of rice auxin response factor OsARF17 by different plant RNA viruses for infection. *Proc. Natl. Acad. Sci. USA* **117**, 9112–9121 (2020).
86. Zhang, H. et al. Different viral effectors suppress hormone-mediated antiviral immunity of rice coordinated by OsNPR1. *Nat. Commun.* **14**, 3011 (2023).
87. Kong, L., Wu, J., Lu, L., Xu, Y. & Zhou, X. Interaction between rice stripe virus disease-specific protein and host PsbP enhances virus symptoms. *Mol. Plant* **7**, 691–708 (2014).
88. Wang, Q. et al. Rice black-streaked dwarf virus P10 promotes phosphorylation of GAPDH (glyceraldehyde-3-phosphate dehydrogenase) to induce autophagy in Laodelphax striatellus. *Autophagy* **18**, 745–764 (2022).
89. Zhang, Y. et al. The circadian-controlled PIF8-BBX28 module regulates petal senescence in rose flowers by governing mitochondrial ROS homeostasis at night. *Plant Cell* **33**, 2716–2735 (2021).
90. Wu, J. et al. Development and use of three monoclonal antibodies for the detection of rice black-streaked dwarf virus in field plants and planthopper vectors. *Virol. J.* **10**, 114 (2013).
91. Ji, X., Wang, L., Zang, D. & Wang, Y. Transcription factor-centered yeast one-hybrid assay. *Methods Mol. Biol.* **1794**, 183–194 (2018).
92. Zhang, D. et al. The MAPK-Alfin-like 7 module negatively regulates ROS scavenging genes to promote NLR-mediated immunity. *Proc. Natl. Acad. Sci. USA* **120**, e2214750120 (2023).
93. Tong, J. et al. ALBA proteins confer thermotolerance through stabilizing HSF messenger RNAs in cytoplasmic granules. *Nat. Plants* **8**, 778–791 (2022).
94. Fu, S. et al. Rice stripe virus interferes with s-acylation of remorin and induces its autophagic degradation to facilitate virus infection. *Mol. Plant* **11**, 269–287 (2018).
95. Kosmacz, M. et al. Protein and metabolite composition of Arabidopsis stress granules. *N. Phytol.* **222**, 1420–1433 (2019).
96. Chen, H. et al. Firefly luciferase complementation imaging assay for protein-protein interactions in plants. *Plant Physiol.* **146**, 368–376 (2008).
97. Zhang, Y. et al. A highly efficient rice green tissue protoplast system for transient gene expression and studying light/chloroplast-related processes. *Plant Methods* **7**, 30 (2011).
98. Kikkert, M. et al. A protoplast system for studying tomato spotted wilt virus infection. *J. Gen. Virol.* **78**, 1755–1763 (1997).

Acknowledgements

We thank Prof. Nan Ma (China Agricultural University) and Prof. Yongliang Zhang (China Agricultural University) for providing pGreenII 0800-LUC and pGreenII 62-SK vectors, Dr. Qiufang Shen (Zhejiang University) for providing 35s-sGFP vector, and Dr. Chenyang Li (Jiangsu Academy of Agricultural Sciences) for providing RSV-infected rice plants. We thank Miss Yunqin Li (Analysis Center of Agrobiology and Environmental Sciences, Zhejiang University) for her assistance during confocal observation, Miss Sanling Wu (Analysis Center of Agrobiology and Environmental Sciences, Zhejiang University) for her assistance with RNA-seq analysis, Miss Shiyan Lu (Analysis Center of Agrobiology and Environmental Sciences, Zhejiang University) for her assistance with SEC-HPLC analyze, Miss Xiaoxiao Feng (the Agricultural Experiment Station, Zhejiang University) for her assistance during glasshouse rice planting. This work was funded by the National Key Research and Development Program of China (Grant no: 2024YFD1400702), the National Natural Science Foundation of China (Grant no: 32472496; Grant No: 31772125), the Earmarked Fund for Modern Agro-industry Technology Research System (Grant no: nycytx-001) and the "Pioneer" and "Leading Goose" R&D Program of Zhejiang (Grant no: 2024SSYS0007).

Author contributions

J.W., X.Z., and T.Z. conceived the research; J.W., X.Z., T.Z., M.Z., and S.F. designed the experiments; M.Z. performed most experiments; S.F., Y.X., L.L., Y.X., D.W., G.S., Z.L., Z.Y., Z.C., F.S., X.Y., L.C., and W.Y. performed additional experiments; M.Z. and J.W. analyzed the data and wrote the paper. All the authors have discussed the results of the manuscript.

Competing interests

The authors declare no competing interests.

Additional information

Supplementary information The online version contains supplementary material available at https://doi.org/10.1038/s41467-025-62395-5.

Correspondence and requests for materials should be addressed to Tong Zhang, Xueping Zhou or Jianxiang Wu.

Peer review information *Nature Communications* thanks Martin Drucker, Souheyla Khechmar, Panagiotis Moschou for their contribution to the peer review of this work. A peer review file is available.